SYNTHESIS AND STUDY OF OPTICAL AND MAGNETIC PROPERTIES OF NANOCRYSTALLINE $Zn_{1-x}Mn_xO$

A DISSERTATION

Submitted in partial fulfillment of the
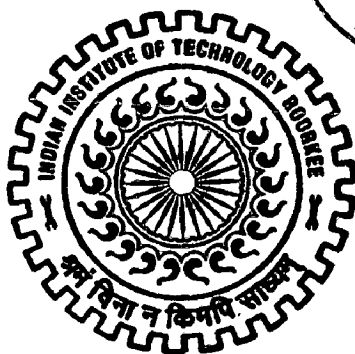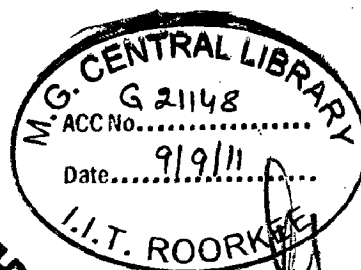*requirements for the award of the degree*
of

MASTER OF TECHNOLOGY

in

NANOTECHNOLOGY

By

SHIVENDRA YADAV

CENTRE OF NANOTECHNOLOGY
INDIAN INSTITUTE OF TECHNOLOGY ROORKEE
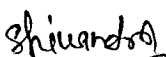ROORKEE - 247 667 (INDIA)
JUNE, 2011

CANDIDATE'S DECLARATION

I hereby declare that the work which is being presented in the dissertation named **"SYNTHESIS AND STUDY OF OPTICAL AND MAGNETIC PROPERTIES OF NANOCRYSTALLINE $Zn_{1-x}Mn_xO$ "** in partial fulfillment of the requirements for the award of the degree of Master of technology submitted in Centre of Nanotechnology, IIT Roorkee is an authentic record of my own work carried out during the period of August, 2010 to June 2011 under the supervision and guidance of Dr. **G.D.Varma**.
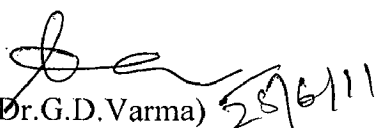
The matter embodied in this project work has not been submitted for the award of any other degree.

Date. 25-06-11

ShivendraYadav

CERTIFICATE

This is to certify that the above statement made by the candidate is correct to the best of my knowledge.

(Dr.G.D.Varma)

Asso. professor

Dept of Physics & Centre of Nanotechnology

Indian institute of technology Roorkee

Roorkee-247667

ACKNOWLEDGEMENT

ABSTRACT

Mn doped ZnO nanocrystalline samples have been synthesized using a simple autocombustion method. The as-synthesized Mn doped ZnO nanocrystals were characterized by X-ray diffraction and scanning electron microscopy. An increase in the hexagonal lattice parameters of ZnO is observed on increasing the Mn concentration. Optical absorption studies show an increment in the band gap with increasing Mn content, and also give evidence for the presence of Mn^{2+} ions in tetrahedral sites. All $Zn_{1-x}Mn_xO$ ($0 < x < 0.20$) samples are paramagnetic at room temperature as find by SQUID measurements even we find room temperature ferromagnetism for low doped Mn-ZnO. However, a large increase in the magnetization is observed below 50 K. This behavior, along with the negative value of the Weiss constant obtained from the linear fit to the susceptibility data below room temperature, indicate ferrimagnetic behavior. The origin of ferrimagnetism is likely to be either the intrinsic characteristics of the Mn doped samples, or due to some spinel-type impurity phases present in the samples that could not be detected.

List of figure

CONTENT:

CHAPTER 1
INTRODUCTION

1.1. DILUTED MAGNETIC SEMICONDUCTORS:

Dilute magnetic semiconductors (DMS) are semiconductors where a fraction of the cations in the lattice are replaced substitutionally by magnetic ions (fig.1). The atomic spin on these magnetic dopants is expected to interact with the carriers in the lattice to bring about global ferromagnetic order in the material.They have unusual magnetic characteristics due to the presence of isolated magnetic ions in semiconducting lattice.

Significant effort was made in trying to develop various DMS candidates as well as in understanding the origin of magnetism in these materials starting from the 1980's.Initial studies focused on II-VI compounds such as CdSe doped with transition metals [1]. DMS were interesting from both a theoretical,as well as a technological stand-point. Unlike metals,semiconductors allow properties such as band gap and carrier concentration to be tailored to fit the application. Further, if the magnetism in the material is related to the carrier concentration, then it might be possible to electrically tune the magnetism. This could lead to a new functionality of gate-controlled ferromagnetism. Although physics of the magnetism was thoroughly investigated in II-VI DMS, they were not suitable for technological applications. One of the reasons for this was that they did not have a mature growth technology. Furthermore, ferromagnetic order could not be achieved at high temperatures in these materials. In fact, the magnetism observed was attributed to spin-glass like frustrated behavior, with very low spin glass transition temperatures.

The area of DMS caught the attention of a much larger research community with the demonstration of magnetic order in Mn-doped InAs and GaAs [2]. Moreover,several curious effects arise from combining magnetism with semiconductors. For instance, in certain systems such as Co-doped TiO_2 [3] or SnO_2 [4] as well as in the case of Gd-doped GaN [5], unusually large magnetic moments per dopant ion have been observed. In order to utilize DMS for technological applications, a sound understanding of the origin of magnetism in these materials is required. Magnetic interactions in solids are discussed in this chapter, as well as the important models used to predict Curie temperatures in prospective DMS candidates.
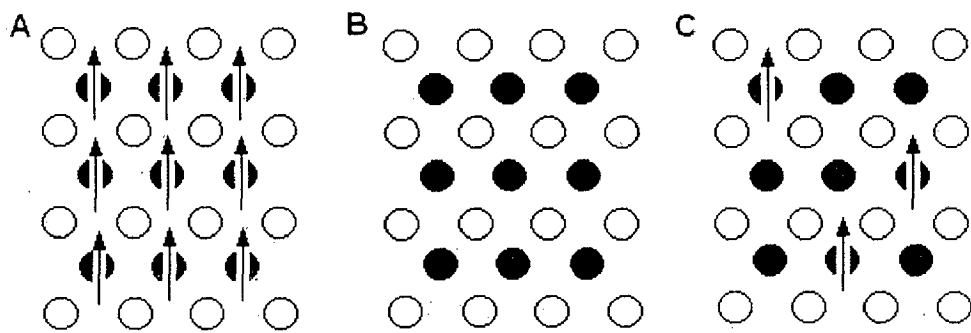
Figure 1: Semiconductor host doped with magnetic ions

Diluted Magnetic Semiconductor (DMSs) makes reference to semimagnetic semiconductors, whose lattice is made up in part of substitution magnetic ions or appropriated rare earth. These semiconductor heterostructures have been intensively studied for many investigators in the world, due to the application in spintronics, which offers big opportunities for the next generation of microelectronic-nanoelectronic devices as well as spin dependent effect.

2

The most structure study today, have been focused to the IV/II ,A TM B alloy (where the TM = $Sc^{2+,}$ $Ti^{2+,}$ $V^{2+,}$ $Cr^{2+,}$ $Mn^{2+,}$ $Fe^{2+,}$ $Co^{2+,}$ Ni^{2+} and Cu^{2+} or rare earth as (Eu, Gd, Er) in which a fraction of the group II sub-lattice are replaced at random by this elements, given rise to localized magnetic moments in the semiconductor host.These diluted magnetic semiconductors of the IV/II ,A TM B type are of interest for several distinct reasons

a) Their ternary nature gives us the possibility of "tuning" the lattice constant and band parameters by varying the composition of the material.

b) The random distribution of magnetic ions over the cation sub-lattice leads to important magnetic effects, e.g., the formation of the spin-glass- like phase at low temperatures.

c) The substitution transition metal ions like Mn atoms in the AIIBIV structure are also characterized by highly efficient electroluminescence, which make dilute magnetic semiconductor alloy important in the context of optical flat panel display application.

d) The spin dependent properties leads to dramatic effects physics, such as the giant Faraday rotation, the magnetic field induce metal-insulator transition, and the formation of bound magnetic polarons.

e) Due of the tenability of their lattice parameter and their energy gaps, the IV/ II, A TM B alloy are excellent candidate for the preparation of quantum wells,superlattices and another configuration that involve band-gap engineering.

1.2. OXIDE-BASED SEMICONDUCTORS:

In contrast to non-oxide semiconductors. the oxide semiconductors have many advantages. Their wide band gap makes them transparent and also suitable for applications with short wavelength. They can be easily grown at low temperature even on

a plastic substrate and are ecologically safe and durable besides being low in cost. In addition, the strong electronegativity of oxygen is expected to produce strong p-d exchange coupling between band carriers and localized spins, and prerequisite for DMS.

1.3. ZnO - based DMS:

Nanostructured ZnO materials have received broad attention due to their distinguished performance in electronic, optics and photonics. Synthesis of ZnO thin film has been received an active field because of their application as sensor, traducers and catalysts. ZnO is a semiconductor material of II-VI compound of the periodic table whose ionicity resides at the borderline between covalent and ionic semiconductor. The electronegative difference between zinc and oxygen produce a high degree of ionicity in its bond, which is considered in ones of the compounds much ionics of this family.
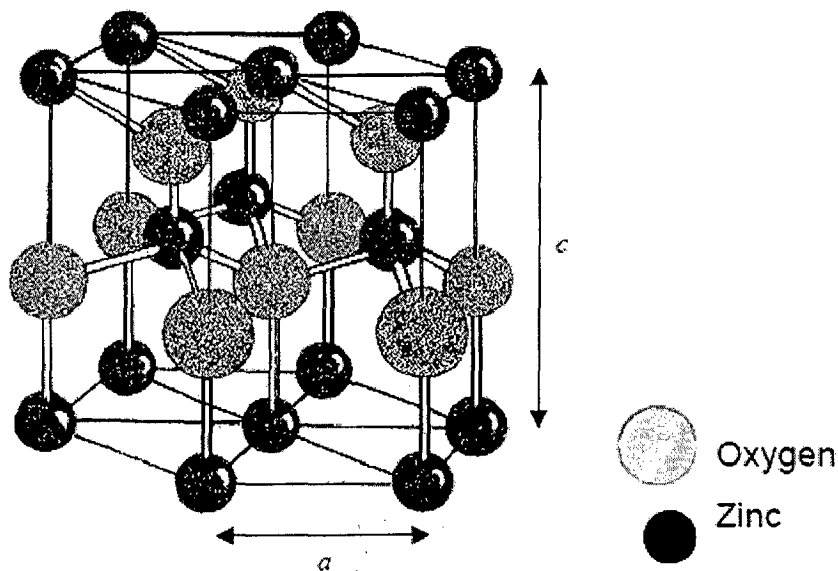
Fig.2.crystal structure of ZnO
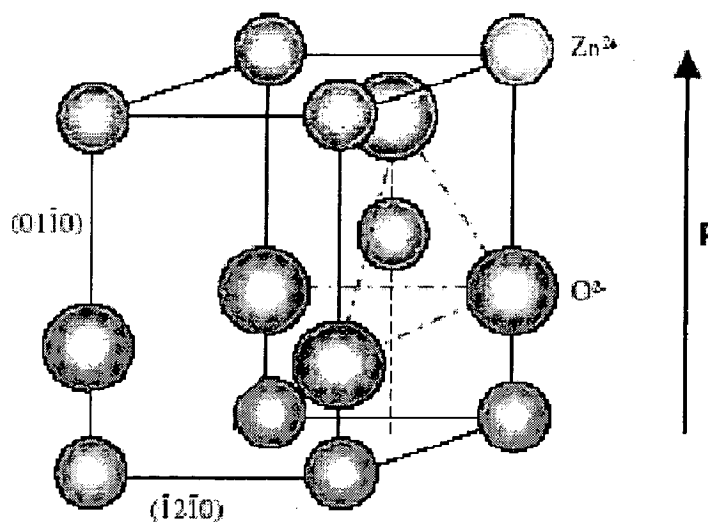
Fig.3.single crystal representation of ZnO

Absence of ferromagnetic behavior was observed at 2 K by H. W. Zhang et al[6]. The magnetization was found to be contributed from both free spin and spins associated with antiferromagnetic cluster. The antiferrromagnetic was confirmed by fitting a Curie-Weiss function.No ferromagnetic behavior has been observed at temperature 5 K in Zn0.93Mn0.07O thin film deposited by RF magnetron sputtering [7]. The Auger spectroscopy showed that Mn is uniformly distributed throughout the film. The ferromagnetic property has been concluded as paramagnetic because the field dependent magnetization can be described well with Curie-Weiss law. Ueda et al [8] prepare by pulsed-laser deposition technique $Zn_{1-x}TM_xO$ (x=0.05-0.25: Mn) thin film, and any evidence of ferromagnetic behavior were not observed. they did not find any ferromagnetism in their Mn- doped ZnO film grown on sapphire substrate using PLD. On

the other hand Jung *et al* [9]. reported on the discovery of ferromagnetism at low temperature in Mn-doped ZnO on epitaxial film prepared by laser molecular-beam epitaxy (LMBE) where the XRD pattern reveal an orientation preferential in the c-axis. Nevertheless the peak position shifted at lower angle when the concentration of manganese increased possibly due to substitution of Mn ions with a large ionic radius of 0.91 Å of for Zn (0.83 Å). The transition temperature obtained from magnetization measurement (M-T at 0.1T) was 30 K and 45 K, for a fraction of dopant of 0.1 and 0.3, respectively. In this research the coercive field (*Hc*) was 300 Oe at 5 K. Production of wurtzite-type tetrapods nanostructure [10] was prepared by evaporation of Zn metal under humid argon flow. After fabrication, Mn was doped into ZnO nanostructures by diffusion at 600^0C. The XRD pattern did not show any extra peak, which indicated the complete formation of structure. Magnetic measurement showed that the sample exhibited very large coercivity *Hc*=5500 Oe at 5.5 K. However, the FC and ZFC measurement at 100 Oe showed a Curie temperature of 43 K, which is consistent with Curie temperature of Mn_3O_4. On the other hand, Secondary Ion Mass Spectrometer (SIMS) confirmed the existence of Zn^{+2} in the band $(Zn,Mn)Mn_2O_4$ which exhibited similar properties to Mn_3O_4, and should be responsible to the magnetism of the Mn-doped ZnO nanostructure. Heo *et al* [11] deposited Mn- doped ZnO by pulse laser deposition on sapphire substrate. They claimed that the saturation magnetization and coercivity of the implanted single-phase film were both a strong function of the initial annealing temperature (600^0C), suggesting that carrier concentration alone could not account for the magnetic properties of ZnO:Mn.The previous result were consistent with the work of TheOdoropulou *et al* [12] who found that FM in ZnO thin films deposited by

reactive magnetron sputtering was strongly dependent of parameters such as growth

temperature, O_2 partial pressure, and type of substrate (only films deposited on Al_2O_3

substrate were FM). Yan *et al* [13] fabricated thin film of $Zn_{1-x}Co_xAl_{.01}O$ with a dopant

concentration 'x' of 0.15 and 0.3 and $Zn_{0.7}(Mn_{0.15}C_{0.15})O$ on Al_2O_3 substrate by pulsed

laser deposition. All three doped ZnO films showed ferromagnetism at RT (290 K). The

same group also reported that the successful doping of Co and (Mn, Co) co-doping in

ZnO without forming second phases could only be realized at a low deposition

temperature (400°C) and low oxygen pressure (5 x10^{-5} Pa) and suggested under high

deposition temperatures and oxygen pressures, cobalt will not substitute Zn in the lattice.

Only few synthesis processes of colloidal nanoparticles have been reported in the

literature. Colloidal nanocrystals should form ideal hosts for strongly-confined artificial

atoms, i.e. configuration of one to a few electrons occupying the conduction energy levels

in the nanocrystal. Such nanocrystals can be obtained in molar quantities by wet chemical

synthesis with increasing control of the size,shape and surface electronic

properties.Gamelin *et al* [14] reported the synthesis of colloidal Mn^{+2}–doped

$ZnO(Mn^{+2}:ZnO)$ quantum dots at room-temperature and the preparation of ferromagnetic

nanocrystalline thin films by hydrolysis and condensation reaction in DMSO under

atmospheric conditions. Gamelin's group proposed that direct chemical syntheses of ZnO

DMSs can provide better control over material composition than is obtained with some

high-temperature vacuum deposition or solid-state synthesis techniques. The same group

reported robust, high-*Tc* in thin films of these nanocrystals prepared by spin coating at

300 K. The corresponding coercivity was 92 Oe, approximately.

1.4. Synthesis of Doped Semiconductor Nanostructures:

The predicted and experimentally observed high ferromagnetic Curie temperature (T_C) in transition metal doped zinc oxide (TM:ZnO) together with the fact that the host material ZnO is currently being ubiquitously applied in electronics, and in chemical and biosensor applications, make this material one of the most promising compounds for the usage in the fast-growing technology of spintronics. The spatial distribution of the TM ion species within, the host semiconductor matrix is essential to the magnetic properties of the system [15]. The physical complexity of real systems due to complicated physics only often makes them too hard of a task for conventional ab initio calculations [16]. One has to therefore insist on avoiding TM ion clustering and formation of magnetic nanoprecipitates in actual materials to be as close as possible to the original theory that caused the ongoing vigor in the field. Different synthesis methods have been applied and will be listed here with their advantages [17]

1.4.1. Thin films deposition:

TM-doped ZnO films are frequently deposited [18] by pulsed laser deposition (PLD), magnetron co-sputtering that can be direct current (dc) reactive [19] and radio-frequency (rf), ultrasonic-assisted solution [20] and plasma enhanced [21], chemical vapor deposition (CVD), combinatorial laser molecular beam epitaxy (laser MBE) [22] , ion-beam sputtering[23] and sol-gel methods [24]. A high degree of ambiguity exists in thin films produced by these methods, such as in the example of Co doped ZnO films that alternatively exhibit room temperature ferromagnetism and room temperature

paramagnetism, the difference being in the synthesis method, PLD or magnetron sputtering.

1.4.2. Solid state reaction methods:

Basic solid state reaction, consisting in the heat treatment of ZnO and transition metal oxide at high temperature has been among the first methods used to produce TM doped ZnO. However,the use of high temperature combined with poor homogeneity of the starting mixture yielded the production of inhomogeneous materials. The results of the magnetic properties of materials produced by solid state reaction are therefore controversial. Peiteado et al. [25] studied the reaction between ZnO and MnOx at different temperatures using the diffusion couple technique. They found that below 973 K no Mn diffusion into ZnO actually occurs, while at the higher temperature Mn^{4+} reduces to Mn^{3+} thereby forming Mn_2O_3. This substantiates the need to develop synthesis based from homogenous starting materials prepared by low temperature process.

1.4.3. Soft chemistry methods:

Numerous soft chemistry processes have been developed to produce at low temperature homogenous precursors aiming at circumventing the diffusion issues of the solid state reaction. As an example, Thota et al. [26] developed zinc oxalate precursors doped with transition metal by adding oxalic acid to ethanolic solution in which Zn and TM acetates have been previously dissolved. This yielded to the gelification of the solution. Once dried, TM doped Zn oxalates are obtained and undergo decomposition to produce TM doped ZnO. Materials obtained by this process have different properties depending on the dopant. In the case of Ni ferromagnetic state was obtained by observing hysteresis loops at 10 K and 320 K. Manganese and cobalt doped ZnO do not reflect any hysteresis loops

9

and their magnetization is found to decrease with Mn or Co content. Schwartz et al.[27] have developed a method of the preparation of colloidal ZnO-diluted magnetic semiconductor quantum dots by alkaline-activated hydrolysis and condensation of

zinc acetate solutions in dimethyl sulfoxide (DMSO).From the electronic absorption spectra and in the ZnO band gap and Co^{2+} ligand field energy regions of the system collected by titration of 0.2 equivalent aliquots of $N(Me)_4OH$ to a DMSO solution of 98 % $Zn(OAc)_2$ / 2 % $Co^{2+}(OAc)_2$ the authors conclude that Co^{2+} ions in solution remain octahedrally coordinated until the nucleation of ZnO crystallites. When Co^{2+} ions bind to the nanocrystal surfaces they do so in tetrahedral geometries either as monomers or within basic acetate clusters. Reaction with $OH-$liberates acetate and yields substitutionally doped Co:ZnO.

Auto-combustion synthes is method have been developed by Deka et al. [28]. High-purity Zn is dissolved in dilute nitric acid and mixed with a water solution of $Co(NO_3)_2 \cdot 6H_2O$. Glycine is added to the solution which is placed on a hot plate until a thick mass is formed. The final solution which was made by adding water solution of glycine to the solution of the metal nitrates was subsequently put on a hot plate till it formed a thick mass that subsequently underwent auto-combustion by the exothermic oxidation of the glycine by the nitrates. A fine powder is obtained.

1.4.4. Co-precipitation methods:

Bouloudenine et al. [29] reported on the preparation of Co doped Zn oxalate by co-precipitation in aqueous medium. Pink oxalate precursors turned green when exposed to high temperature.Magnetization measurements reveal a paramagnetic behaviour. Numerous different organometallic salts , such as acetates [30] and citrates [31] prepared

by co-precipitation have also been used to produce TM doped ZnO. However, for the same nominal composition different types of magnetic behaviour have been observed depending on the decomposition as well as on the choice of the precursor salt used [32].

1.4.5. Drawbacks of the synthesis methods:

There are several drawbacks of the synthesis methods which corroborate the inconsistency listed previously in the magnetic properties of TM doped ZnO. The high temperature methods are found to be inadequate in producing single-phase with homogenously distributed TM species $Zn_{1-x}TMxO$ [33, 34, 35] often leading to the formation of TM in higher oxidation states and impurities. This is in a big part due to poorly mixed starting materials. As previously mentioned the mixture quality of the starting materials is the key to obtaining homogeneous TM doped ZnO. Although it has been dramatically improved by the use of organometallic precursors, this is not believed to be adequate. Because of the low intrinsic oxygen content of the organometallic salts, oxygen is usually added to complete the oxidation of organic carbon during the decomposition.Other drawbacks exist. First, organic precursors undergo multistep decomposition processes,forming intermediate organic salts having dissimilar Zn or TM solubilities compared to the original precursor material(s). Second, the character of different decomposition steps is heavily influenced by environmental factors like the atmosphere, and so can change between endothermic and exothermic [36, 37]. As a result, sample temperature may fluctuate dramatically during the decomposition. The variations of Zn and TM solubility within the organic matrix, combined with temperature fluctuations, can yield chemical gradients within the final products, and, hence, the formation of TM rich impurities [38].

1.5. Properties of Doped Nanoparticles:

Recently, transition-metal (TM)-doped ZnO has been extensively investigated as a promising dilute magnetic semiconductor (DMS) for implementing spintronic device concepts. The ferromagnetism(FM) measurements at various temperatures have been reported in Co-,Ni-,Mn-, and Fe-doped ZnO thin films[38]as well as nanostructures,[39] and room temperature FM has been experimentally demonstrated in Co or Mn-doped ZnO thin films or nanostructures.[40] For example, Djerdj et al.[41] demonstrated that the Co-doped ZnO powders are indeed ferromagnets with a Curie temperature above room temperature (RT) and the Mn-doped samples show antiferromagnetic correlations with a possible transition to an antiferromagnetic ground state below $T_N \approx 10$ K. Coey et al.[42] proposed that the ferromagnetic exchange is mediated by shallow donor electrons that form bound magnetic polarons that overlap to create a spinsplit impurity band. However, a doped ZnO nanostructure by a controllable method is difficult to prepare [43,44]. Most of the researchers reported that they had difficulties in controlling the structure and the composition of the doped ZnO NWs or nanorod arrays. Moreover, there is a great deal of controversy about whether TM-doped ZnO has room temperature FM, and the research on the electrical properties of TM-doped ZnO arrays has scarcely been reported, which could limit the applications of ZnO arrays. In addition, the majority of magneto transport studies on DMS materials have been reported in either the bulk or thin film forms. There are far fewer reports of spin transport in one dimensional DMS materials, such as nanowires [45]. In TM-doped ZnO nanostructures, some work have concentrated on the growth of Co or Mn respectively doped ZnO nanostructures and characterization of their structural, magnetic, and electrical properties [46-47].

Obviously, the use of carrier spin, in addition to the charge, appears very promising for the emergence of polarized emitters.[48] A key requirement for the use of spin based electronic devices (spintronic) is the persistence of ferromagnetism above room temperature. Early studies on manganese doped ZnO have shown room temperature ferromagnetism, and ZnO has one of the few oxides scheduled to be used in polarized emitters. The fundamental origin of the observed magnetic behavior has attracted much attention since 2000. In an extremely quoted paper, T. Dietl et al. reported a theoretical study on the Curie temperature of ferromagnetic DMS.[49] Interestingly, the experimental study of manganese doped zinc telluride supported the calculations and room temperature ferromagnetism was predicted for p-type manganese doped ZnO (and n-type cobalt doped ZnO).The revival of this already old field mainly occurs due to the assumption that room temperature ferromagnetism is indeed promoted by the semiconductor charge carriers, based on the so-called Zener model adapted to DMS. However, many of the claims of high-temperature ferromagnetism in DMS systems are controversial[50]. The high temperature synthesis process may explain the tendency of these materials to phase-separate into a ZnO matrix with transition metal inclusions.[51] The semiconducting properties would then originate from the matrix and the magnetic properties from the clusters. In addition, the exact origin of the observed magnetic behavior in these systems depends on the dopant/matrix system and the carrier concentration and thus on synthetic conditions.

Consequently, the main point of any new study relies on the exclusion of any secondary phase as origin for ferromagnetism. Mn doped ZnO nanostructures from physical routes have been widely studied as thin films, nanorods,[52] or nanowires. Similar studies have

been carried out on Co doped ZnO with thin films,[53] nanorods,[54,55] and nanowires. One-dimensional systems are particularly interesting for the study of DMS.

1.5.1. ZnO:Mn

Zinc oxide is a wide bandgap material that can crystallizein a cubic zinc blend (wurtzite) structure [56]. The direct bandgap in a bulk solid is 3.35 and 3.42 eV at 300 and 0 K, respectively. Doped Zinc oxide also has been considered as a low voltage, stable phosphor material for flat panel display application, thin films have interesting optical and magnetic properties. Although optical and structural properties of undoped ZnO nanoparticles have been reported in the past, there, is little research on doped ZnO nanoparticles.However, it is one of the likely candidates for DMS. Therefore, it would be worthwhile in the future to investigate nanoparticles of ZnO and doped ZnO as already begun by some groups. Luminescence in manganese and europium-doped ZnO nanoparticles has been reported by Bhargava et al. [57]. Sapra et al. [58] have synthesized $Zn_{1-x}Mn_xO$ nanoparticles and investigated the structure and optical properties.The particle size was 4-7 nm as determined by X-ray diffraction and bandgap measurement.

1.6. Application:

The introduction of computers to the world's stage has had such huge influence on the everyday life that it is difficult to grasp a life without computers. No wonder than the old Olympic motto of Citius, Altius, Fortius is being modified to be Citius, Minor, Fortius, where "smaller" refers to the size of the electronic components. The working principle behind the new computers, including I-Pad, is based on the silicon semiconductor technology and the principle of transistor, transfer resistor, that has been developing

since the 1950s. The silicon transistor/integrated circuit technology is working using the fundamental property of the electron charge. Electrons however have an additional fundamental property, *spin* that can have the value of 1/2 or -1/2. If one would be able to control the spin states of the spins one would be in position to perform calculations several orders of magnitude faster than in conventional electronics, and the leap in power/size ratio would far supersede the leap that I-Pad made these days. The spintronics has already made its way to I-Pad through its hard disk data storage drive using giant magnetoresistance effect, which is the 20-80 % change in resistance between the cases when the adjacent magnetic layers are under an applied field and without the applied field, respectively. Hence, by applying the magnetic field, one has the change of one to zero and a unit of information is created.

The spin of the electron is hence used in hard-disk technology, yet the challenge that remains is developing a spintronics device out of semiconductors, which could make the logical elements in computers function on the principle of measuring the spin state of the electrons and not whether the current is on or off. This could finally achieve a computer that could boot-up instantaneously or be in stand-by state without any power needed , a significant step forward from the computers that we know today.

Spintronics is a novel technology based on usage of spins as information units that could possibly revolutionize the information technology as we know it today. Modern technologies are often developed in parallel or directly through the development of structures based on their flagship materials. The revolution of electronics with Si, optoelectronics with GaAs and display technology with liquid crystals are one of many examples. Spintronics is not an exception to this rule, scientists being constantly in search

for suitable materials to achieve the goal of computing with individual spins. Materials for spintronics in general have to have the potential for amplification of spin-dependent properties. Diluted magnetic semiconductors are materials with properties such as giant Faraday rotation, the change in polarization of light when acting with the magnetic field and extremely large Zeeman splittings, the splittings of the energy states of the electrons in presence of a strong magnetic field, of both the band and impurity levels. ZnO by itself is already a promising material as it already easily finds its place in many demanding applications. It is used as a varistor, a variable resistor material used to e.g. protect sensitive pieces of electronic equipment by shunting the circuits [58], as a piezoelectric material, a material capable of generating electric potential when dangerously high current levels are present, etc. It can also be used as a nano-cantilever in Atomic Force Microscope (AFM) [59]. It is as well a high-k dielectric, i.e. a material with a high dielectric constant k compared to SiO2 meaning that it could replace the silicon dioxide gate in conventional transistors and contribute to miniaturization of the electronic components which is essential to the optimization of their performance. In addition to all the mentioned characteristics, doping of n-doped ZnO with Co, Ni, V and Fe are predicted to render it ferromagnetic [60], while doping of p-doped ZnO with Mn serves to the same effect [61]. Ferromagnetic semiconductors are essential candidates to make some or all of the (source, drain, channel,gate) components of a conventional spin-field effect transistor (spin-FET) [62]. One more reason then, to embark on the journey of ZnO, DMS and spintronics.

CHAPTER 2
EXPERIMANTAL TECHNIQUES

2.1. Materials and Instruments used:

Chemical salts and Reagents used:

- Zinc Metal Powder(S-D-Fine)

- Manganise Metal Powder(Himedia)

- Glycine Powder(Thomas Baker)
- Nitric Acid(Rankem)
- Acetone(Thomas Baker)
- Millipore(Elix)

2.2. Instruments and Equipments used:

- Bruker X-8, X-Ray diffraction instrument

- FEI Quanta200f for FESEM and EDAX

- Elix Millipore for Distilled water

- Super-conducting quantum interference device(SQUID)

- Vibration sample magnetometer(PAR 155 Model)

- UV-vis spectrophotometer(Varian Carry 500 Model)

- UV-vis diffuse reflectance spectrophotometer(Varian Carry 500 Model)

- Photolumniscence spectrometer(Simartdzu 5310 model)

- Hot plate heater(Safex)

- Ultrasonic(Equitron

17

2.3. Characterisation techniques:

2.3.1. X-Ray Diffraction Analysis:
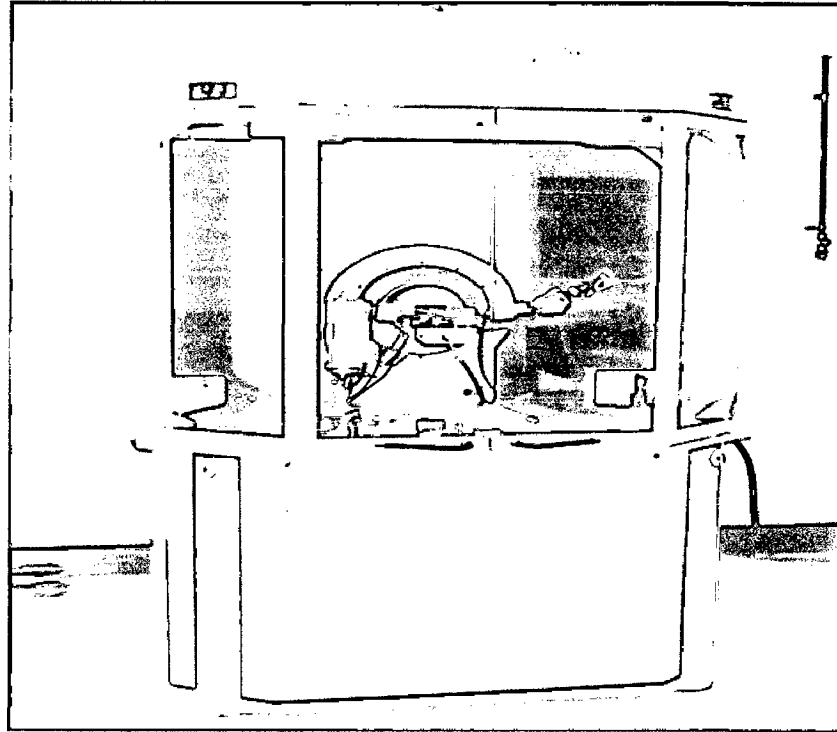
Fig.4.X-Ray Diffractometer

X-ray powder diffraction (XRD) is a rapid analytical, non-destructive technique primarily used for phase identification of a crystalline material and can provide information on unit cell dimensions, chemical composition, and physical properties of materials. This technique is based on observing the scattered intensity of an X-ray beam hitting a sample as a function of incident and scattered angle, polarization, and wavelength or energy. Computer analysis of the peak positions and intensities associated with this pattern enables qualitative analysis, lattice constant determination and/or stress determination of

the sample. Qualitative analysis may be conducted on the basis of peak height or peak area. The peak angles and profiles may be used to determine particle diameters and degree of crystallization, and are useful in conducting precise X-ray structural analysis. The identification of single or multiple phases in an unknown sample is the main application of X-ray powder diffractometry.

When a monochromatic X-ray beam with wavelength lambda is projected onto a crystalline material at an angle theta, diffraction occurs only when the distance traveled by the rays reflected from successive planes differs by a complete number n of wavelengths.

Bragg's Law

By varying the angle theta, the Bragg's Law conditions are satisfied by different d-spacings in polycrystalline materials. Plotting the angular positions and intensities of the resultant diffracted peaks of radiation produces a pattern, which is characteristic of the sample. Where a mixture of different phases is present, the resultant diffractogram is formed by addition of the individual patterns. The diffraction data is compared against a database maintained by International Centre for Diffraction Data.

X-ray diffractometers consist of three basic elements: an X-ray tube, a sample holder, and an X-ray detector. X-rays are generated in a cathode ray tube by heating a filament to produce electrons, accelerating the electrons toward a target by applying a voltage, and bombarding the target material with electrons. When electrons have sufficient energy to dislodge inner shell electrons of the target material, characteristic X-ray spectra are

produced. These spectra consist of several components, the most common being K_α and K_β. K_α consists, in part, of $K_{\alpha 1}$ and $K_{\alpha 2}$.

Copper is the most common target material for single-crystal diffraction, with Cu K_α radiation = 0.5418Å. These X-rays are collimated and directed onto the sample. As the sample and detector are rotated, the intensity of the reflected X-rays is recorded. When the geometry of the incident X-rays impinging the sample satisfies the Bragg Equation, constructive interference occurs and a peak in intensity occurs. A detector records and processes this X-ray signal and converts the signal to a count rate which is then output to a device such as a printer or computer monitor. The geometry of an X-ray diffractometer is such that the sample rotates in the path of the collimated X-ray beam at an angle θ while the X-ray detector is mounted on an arm to collect the diffracted X-rays and rotates at an angle of 2θ. The instrument used to maintain the angle and rotate the sample is termed a goniometer.

2.3.2. FESEM Analysis:
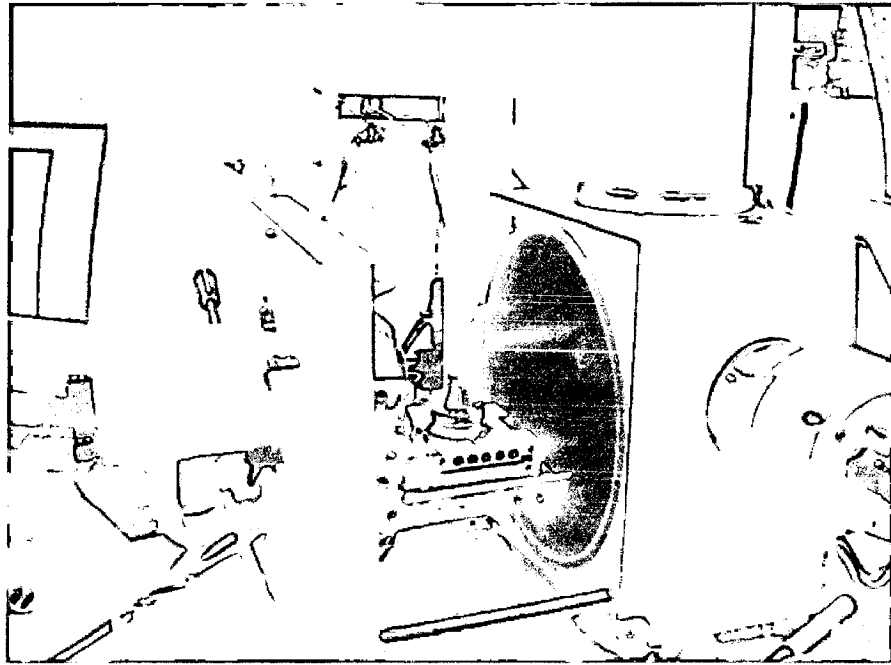
Fig.5. FE-SEM

FESEM stands for Field emission scanning electron microscope. The FESEM is a microscope that uses electrons instead of light to form an image. Since their development in the early 1950's, scanning electron microscopes have developed new areas of study in the medical and physical science communities. The FESEM has allowed researchers to examine a much bigger variety of specimens.

The scanning electron microscope has many advantages over traditional microscopes. The FESEM has a large depth of field, which allows more of a specimen to be in focus at one time. The FESEM also has much higher resolution, so closely spaced specimens can be magnified at much higher levels. Because the FESEM uses electromagnets rather than lenses, the researcher has much more control in the degree of magnification. All of these

advantages, as well as the actual strikingly clear images, make the scanning electron microscope one of the most useful instruments in research today.

Various parts of FESEM:

The sample is fixed with conductive tape on a metallic sample block. Non-conductive specimens are coated with a nanometer thin-layer of metal to facilitate emission and flow of electron in the surface. The metal block is crewed on a sample holder and positioned in the pre-vacuum chamber, an intermediate chamber with a front and a rear lid. This chamber acts as a lock. When the vacuum in this space is low enough the shutter to the high vacuum (lowest pressure) is opened and the object is shifted with a long rod into the object chamber on a rails just under the column. In order to ease the positioning a one can observe the inner view of the object chamber with an infra red camera. The object chamber is the place where the sample is irradiated by the electron beam. The position of the sample stage can be adjusted in height (z-navigation) and horizontally (x-y navigation). The topographical scanning electron imaging requires a secondary electrons detector, like in a normal SEM there is a control panel, a monitor for the operation of the device and one showing the SE images. A separate EDS detector allows one to capture the X-ray scanning and there is another back-scattered electron detector. In this chamber in the heart of the electron microscope the vacuum is extremely low: 10^{-6}mBar (thus 1:1.000.000.000 the normal atmospheric pressure; vacuum display = 16; around the electron gun the vacuum is even two orders of magnitude lower). The need for such extreme vacuum is that collision of bombarding electrons from the beam with gas

22

molecules in the column would result in heat production. Cooling and supply of electric power are required in order to maintain this extreme vacuum.

Under vacuum, electrons generated by a Field Emission Source are accelerated in a field gradient. The beam passes through Electromagnetic Lenses, focussing onto the specimen. As result of this bombardment different types of electrons are emitted from the specimen. A detector catches the secondary electrons and an image of the sample surface is constructed by comparing the intensity of these secondary electrons to the scanning primary electron beam. Finally the image is displayed on a monitor.

In SEM the image is formed from secondary electrons that have been dislocated at the surface of the scanned sample by bombarding primary electrons from the electron gun. Those ejected electrons are captured by a detector and the information is converted into an electric signal, amplified and digitalized. The result is a topographical image of the surface of the object, e.g. the surface of a metal coating or lamellae of fish gills (see example here below). Besides secondary electrons, radiation (in particular X-rays and cathodoluminescence in typical samples) as well as back-scattered and so-called Auger electrons with an own energy level are produced upon interaction of atoms in the surface layer of the sample with the primary electron beam. These emission signals, which contain information among others on the element composition of the upper layer, can be received by selected detectors, as is the case in EDAX microscopes for example, and combined with the topographical image.

Besides, there are scanning electron microscopes which are equipped with EDS (Energy Dispersed Spectroscopy) or EDAX (Energy-Dispersed Analysis of X-rays) detectors that

capture the emitted X-ray. With such instruments it is possible to determine which elements are present in the surface layer of the sample (at a depth in the micrometer range) and where these elements are present ("mapping technique"). This particular microscope also allows one to capture directly reflected electrons, the so-called back scattered electrons, from which one can obtain a global appreciation whether one or several elements are present in the surface layer of the sample. Also the so-called Auger electrons, which are emitted just under the surface, provide information about the nature of the atoms in the sample.

SAMPLE PREPARATION FOR FESEM:

Because the SEM utilizes vacuum conditions and uses electrons to form an image, special preparations must be done to the sample. All water must be removed from the samples because the water would vaporize in the vacuum. All metals are conductive and require no preparation before being used. All non-metals need to be made conductive by covering the sample with a thin layer of conductive material. This is done by using a device called a "sputter coater."

The sputter coater uses an electric field and argon gas. The sample is placed in a small chamber that is at a vacuum. Argon gas and an electric field cause an electron to be removed from the argon, making the atoms positively charged. The argon ions then become attracted to a negatively charged gold foil. The argon ions knock gold atoms from the surface of the gold foil. These gold atoms fall and settle onto the surface of the. sample producing a thin gold coating.
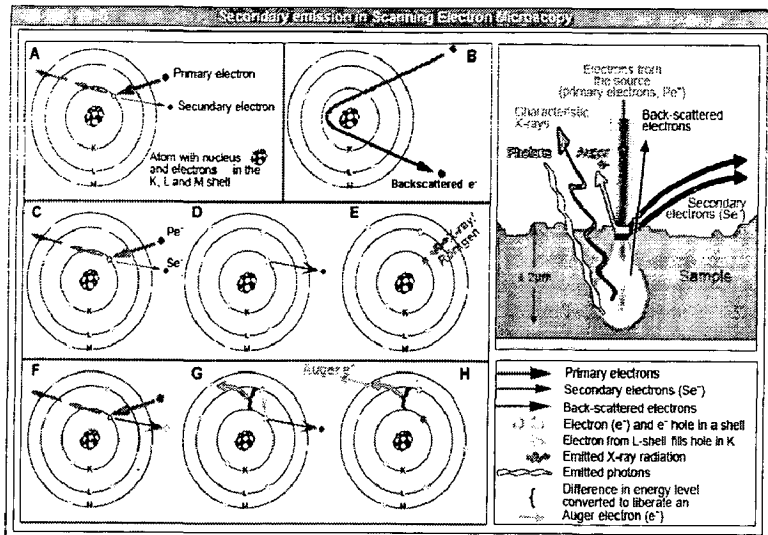
Fig.6. Emissions in SEM

A: The bombarding electrons (=primary electrons) can penetrate in the electron shells of the atoms composing the surface of the sample. The energy (negative charge, mass, velocity) of these incident electrons can be converted to eject local electrons, so-called secondary electrons, from the shells of the atoms in the surface of the specimen. This information cab ne utilized to reconstruct a detailed topographical image of the sample (SEI = Secondary Electrons Imaging). The final image looks like a shadow-cast photograph of the surface of the sample. This record of the morphology is the best-known application of a scanning electron microscope.

B: Primary electron can also be reflected by atoms at about 10-100 nanometre depth at the surface. These so-called "back-scatter" conserve their energy at incidence, but their direction of propagation has been modified upon interaction. One can obtain a rough representation whether the surface of the sample is constituted of a single or multiple elements.

C, D, E: at the surface of the sample electrons in the deeper electron shells (shell K in **C**) can be ejected by primary electrons (Pe-indicated in red), resulting in an electron hole. When this lower-shell position is filled by an electron from a higher shell (green arrow in **D**) energy is released. This can be as light (photons; the phenomenon is also called cathode luminescence) or as X-ray. Because each element emits an own characteristic energy value, the elements present in the micrometer range depth of the sample can be determined. See example here below.

F, G, H: another phenomenon is that the energy released upon filling a hole in the K shell by an electron from the L shell is used to expulse an electron from the external M shell: a so-called Auger electron. The released energy is characteristic for the type of atom. Auger electrons are produced in the outermost surface layer (at nanometer depth) of the sample.

EDAX Analysis:

Energy dispersive X-ray spectroscopy (EDS) is an analytical technique used for the elemental analysis or chemical characterization of a sample. It is one of the variants of XRF. As a type of spectroscopy, it relies on the investigation of a sample through interactions between electromagnetic radiation and matter, analyzing x-rays emitted by the matter in response to being hit with charged particles. Its characterization capabilities are due in large part to the fundamental principle that each element has a unique atomic structure allowing x-rays that are characteristic of an element's atomic structure to be identified uniquely from each other.

To stimulate the emission of characteristic X-rays from a specimen, a high energy beam of charged particles such as electrons or protons, or a beam of X-rays, is focused into the sample being studied. At rest, an atom within the sample contains ground state (or unexcited) electrons in discrete energy levels or electron shells bound to the nucleus. The incident beam may excite an electron in an inner shell, ejecting it from the shell while creating an electron hole where the electron was. An electron from an outer, higher-energy shell then fills the hole, and the difference in energy between the higher-energy shell and the lower energy shell may be released in the form of an X-ray. The number and energy of the X-rays emitted from a specimen can be measured by an energy dispersive spectrometer. As the energy of the X-rays is characteristic of the difference in energy between the two shells, and of the atomic structure of the element from which they were emitted, this allows the elemental composition of the specimen to be measured.

2.3.3. UV-Vis Spectrophotometer:

Many molecules absorb ultraviolet or visible light. Absorbance is directly proportional to the path length, b, and the concentration, c, of the absorbing species." Beer's Law states that $A = ebc$, where e is a constant of proportionality, called the absorbtivity". Different molecules absorb radiation of different wavelengths. An absorption spectrum will show a number of absorption bands corresponding to structural groups within the molecule. Figure 7. shows the Varian Cary 5000 model of UV-Vis spectrophotometer.

2.3.4. Diffuse reflectance spectroscopy:

Diffuse reflection is a process whereby light reflected from an object strikes other objects in the surrounding area, illuminating them. Diffuse inter reflection specifically describes light reflected from objects which are not shiny or specular.

Diffuse reflectance is an excellent sampling tool for powdered materials in the mid-IR and NIR ranges. It can also be used for analysis of intractable solid samples. As with transmission analysis, samples to be run by diffuse reflectance are generally mixed with barium sulphide prior to sampling. Diffuse reflectance is an excellent sampling technique as it eliminates the time-consuming process of pressing pellets for transmission measurements. Diffuse reflectance can also be used to study the effects of temperature and catalysis by configuring the accessory with a heating chamber.

2.3.5. Fluorescence spectroscopy:

Fluorescence spectroscopy is a type of electromagnetic spectroscopy which analyzes fluorescence from a sample. It involves using a beam of light, usually ultraviolet light, that excites the electrons in molecules of certain compounds and causes them to emit light of a lower energy, typically, but not necessarily, visible light. A complementary technique is absorption spectroscopy.

To stimulate the emission of characteristic X-rays from a specimen, a high energy beam of charged particles such as electrons or protons, or a beam of X-rays, is focused into the sample being studied. At rest, an atom within the sample contains ground state (or unexcited) electrons in discrete energy levels or electron shells bound to the nucleus. The incident beam may excite an electron in an inner shell, ejecting it from the shell while creating an electron hole where the electron was. An electron from an outer, higher-energy shell then fills the hole, and the difference in energy between the higher-energy shell and the lower energy shell may be released in the form of an X-ray. The number and energy of the X-rays emitted from a specimen can be measured by an energy dispersive spectrometer. As the energy of the X-rays is characteristic of the difference in energy between the two shells, and of the atomic structure of the element from which they were emitted, this allows the elemental composition of the specimen to be measured.

2.3.3. UV-Vis Spectrophotometer:

Many molecules absorb ultraviolet or visible light. Absorbance is directly proportional to the path length, b, and the concentration, c, of the absorbing species." Beer's Law states that $A = ebc$, where e is a constant of proportionality, called the absorbtivity". Different molecules absorb radiation of different wavelengths. An absorption spectrum will show a number of absorption bands corresponding to structural groups within the molecule. Figure 7. shows the Varian Cary 5000 model of UV-Vis spectrophotometer.

2.3.4. Diffuse reflectance spectroscopy:

Diffuse reflection is a process whereby light reflected from an object strikes other objects in the surrounding area, illuminating them. Diffuse inter reflection specifically describes light reflected from objects which are not shiny or specular.

Diffuse reflectance is an excellent sampling tool for powdered materials in the mid-IR and NIR ranges. It can also be used for analysis of intractable solid samples. As with transmission analysis, samples to be run by diffuse reflectance are generally mixed with barium sulphide prior to sampling. Diffuse reflectance is an excellent sampling technique as it eliminates the time-consuming process of pressing pellets for transmission measurements. Diffuse reflectance can also be used to study the effects of temperature and catalysis by configuring the accessory with a heating chamber.

2.3.5. Fluorescence spectroscopy:

Fluorescence spectroscopy is a type of electromagnetic spectroscopy which analyzes fluorescence from a sample. It involves using a beam of light, usually ultraviolet light, that excites the electrons in molecules of certain compounds and causes them to emit light of a lower energy, typically, but not necessarily, visible light. A complementary technique is absorption spectroscopy.

To stimulate the emission of characteristic X-rays from a specimen, a high energy beam of charged particles such as electrons or protons, or a beam of X-rays. is focused into the sample being studied. At rest, an atom within the sample contains ground state (or unexcited) electrons in discrete energy levels or electron shells bound to the nucleus. The incident beam may excite an electron in an inner shell, ejecting it from the shell while creating an electron hole where the electron was. An electron from an outer, higher-energy shell then fills the hole, and the difference in energy between the higher-energy shell and the lower energy shell may be released in the form of an X-ray. The number and energy of the X-rays emitted from a specimen can be measured by an energy dispersive spectrometer. As the energy of the X-rays is characteristic of the difference in energy between the two shells, and of the atomic structure of the element from which they were emitted, this allows the elemental composition of the specimen to be measured.

2.3.3. UV-Vis Spectrophotometer:

Many molecules absorb ultraviolet or visible light. Absorbance is directly proportional to the path length, b, and the concentration, c, of the absorbing species." Beer's Law states that $A = ebc$, where e is a constant of proportionality, called the absorbtivity". Different molecules absorb radiation of different wavelengths. An absorption spectrum will show a number of absorption bands corresponding to structural groups within the molecule. Figure 7. shows the Varian Cary 5000 model of UV-Vis spectrophotometer.
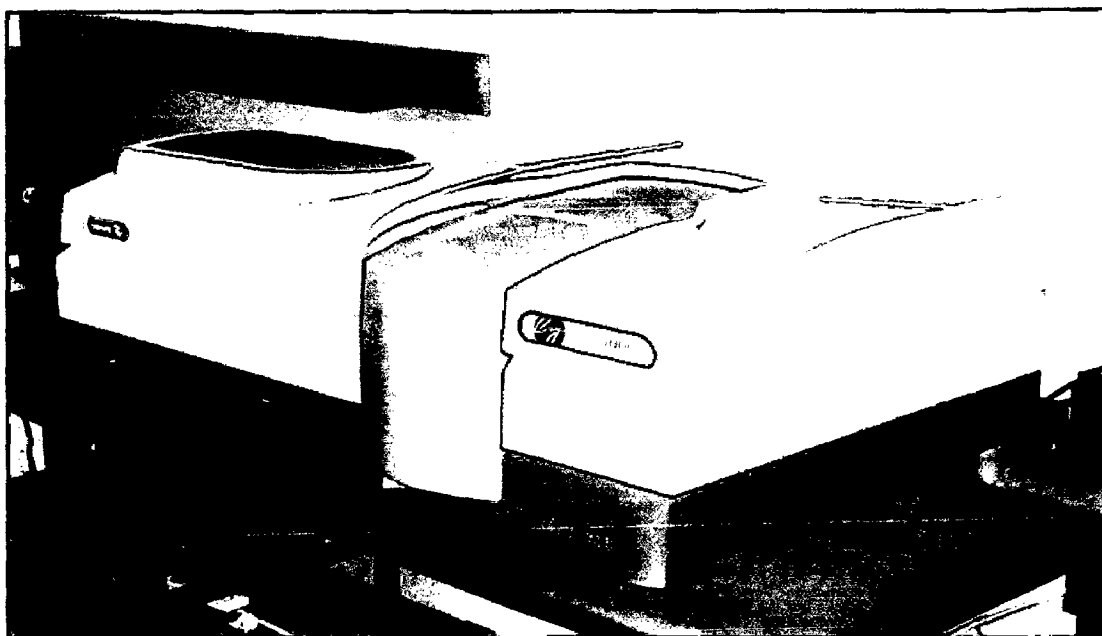
Fig.7.Varian Cary 5000 model of UV-Vis Spectrophotometer

Basic principle - In UV spectroscopy the sample is irradiated with UV radiation, if a particular electronic transition matches the energy of certain band of UV it will be absorbed the remaining UV light passes through the sample and is observed. A spectrum is obtained with gaps at these discrete energies this is absorption spectrum. UV-Vis spectroscopy is routinely used in analytical chemistry for the quantitative determination of different analytes such as transition metal ions, highly conjugated organic compounds and biological macromolecules.

Instrumentation- Instrument consists of a source to emit UV and visible radiation, wavelength selector (monochromator), sample container and signal process and detector. The electrical excitation of deuterium or hydrogen at low pressure produces a continuous UV spectrum. Source of visible radiation is tungsten filament lamp. Polychromatic radiation obtained from UV and visible source enters the monochromator through the

28

entrance slit. The beam is collimated, and then strikes the dispersing element at an angle.

The beam is split into its component wavelengths by the grating or prism. By moving the

dispersing element or the exit slit, radiation of only a particular wavelength leaves the

monochromator through the exit slit. The containers for the sample and reference solution

must be transparent to the radiation which will pass through them. Quartz or fused silica

cuvettes are required for spectroscopy in the UV region. These cells are also transparent

in the visible region. Silicate glasses can be used for the manufacture of cuvettes for use

between 350 and 2000 nm. The photomultiplier tube is a commonly used detector in UV-

Vis spectroscopy. Simple schematic diagram of UV-Vis spectroscopy is shown in figure
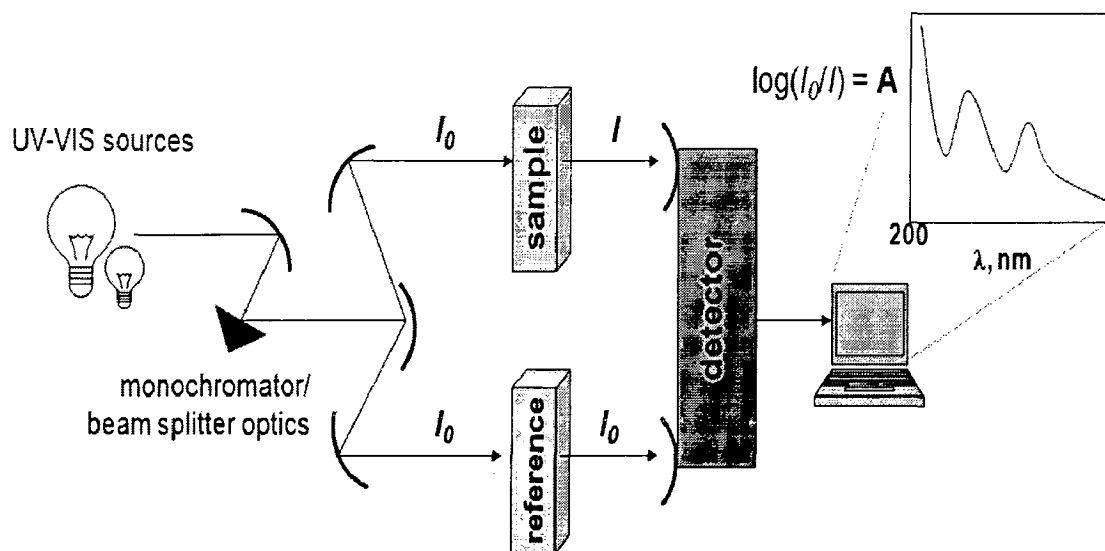

Fig.8. Schematic setup of UV-Vis spectrophotometer

2.3.4. Diffuse reflectance spectroscopy:

Diffuse reflection is a process whereby light reflected from an object strikes other objects in the surrounding area, illuminating them. Diffuse inter reflection specifically describes light reflected from objects which are not shiny or specular.

Diffuse reflectance is an excellent sampling tool for powdered materials in the mid-IR and NIR ranges. It can also be used for analysis of intractable solid samples. As with transmission analysis, samples to be run by diffuse reflectance are generally mixed with barium sulphide prior to sampling. Diffuse reflectance is an excellent sampling technique as it eliminates the time-consuming process of pressing pellets for transmission measurements. Diffuse reflectance can also be used to study the effects of temperature and catalysis by configuring the accessory with a heating chamber.

2.3.5. Fluorescence spectroscopy:

Fluorescence spectroscopy is a type of electromagnetic spectroscopy which analyzes fluorescence from a sample. It involves using a beam of light, usually ultraviolet light, that excites the electrons in molecules of certain compounds and causes them to emit light of a lower energy, typically, but not necessarily, visible light. A complementary technique is absorption spectroscopy.
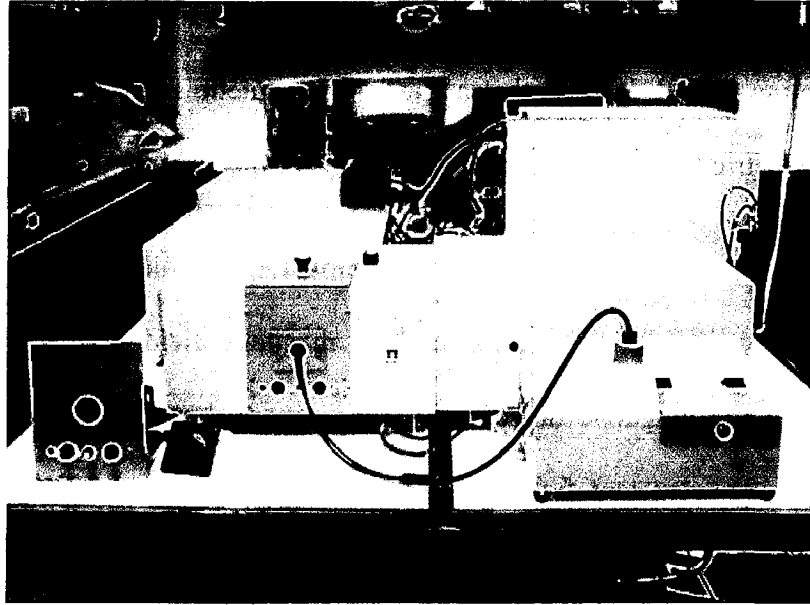
Fig.9.Fluorescene Spectroscopy

2.3.6. Vibrating sample magnetometer (VSM)

VSM is a scientific instrument that measures magnetic properties. It was invented in 1955 by Simon Foner at Lincoln Laboratory MIT. A VSM is used to measure the magnetic behaviour of magnetic materials. A number of magnetic properties used to characterize the different magnetic nanoparticles are the type, strength and direction of remanent magnetization. These can be used to identify the remanence carrier and the (magnetic) domain type of the particles viz. multi-domain (MD), single domain (SD); pseudo single domain (PSD) and superparamagnetic (SP). Usually the particle size decreases in this order.

Basic Principle - A vibrating sample magnetometer (VSM) operates on Faraday's Law of Induction, which tells us that a changing magnetic field will produce an electric field. This electric field can be measured in terms of the changing magnetic field.

A VSM operates by first placing the sample to be studied in a constant magnetic field. If the sample is magnetic, this constant magnetic field will magnetize the sample by aligning the magnetic domains, or the individual magnetic spins, with the field. The stronger the constant field, the larger the magnetization will be. The magnetic dipole moment of the sample will create a magnetic field around the sample, sometimes called the magnetic stray field. As the sample is moved up and down, this magnetic stray field is changing as a function of time and can be sensed by a set of pick-up coils [63]. Figure.10. shows the PAR 155 model of vibrating sample magnetometer
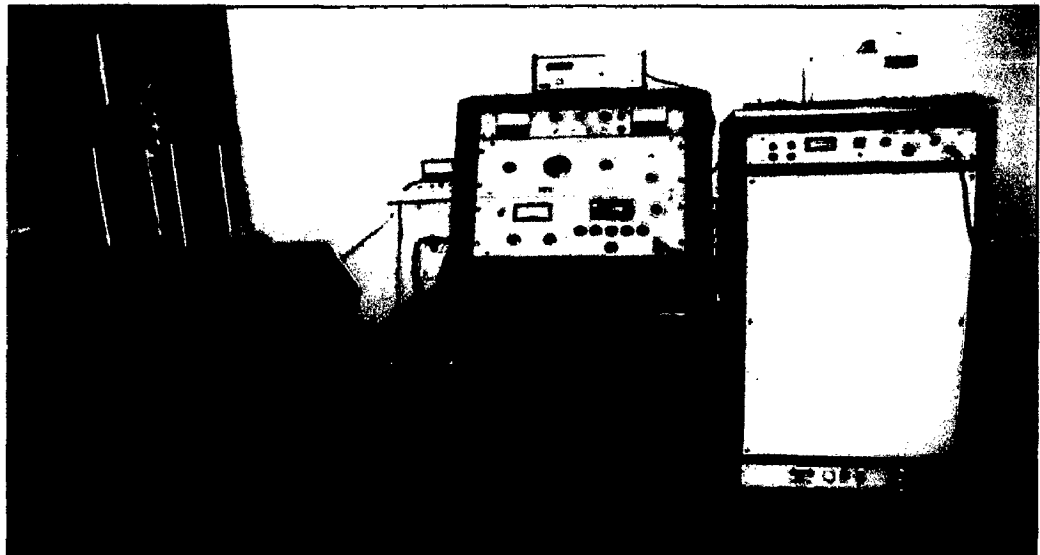

Fig.10. PAR 155 Model of Vibrating Sample Magnetometer

2.3.7. SQUID CHARACTERIZATION

The magnetization curves were measured using a commercial SQUID (Superconducting Quantum Interference Device) magnetometer Quantum Design MPMS. This piece of equipment allows a base temperature of 2 K and a maximum magnetic field of 7 Tesla. The SQUID magnetometer (Figure 11) is the most sensitive device available for measuring magnetic fields, and, although the SQUID in the MPMS is the reason for the instrument's remarkable sensitivity, it does not detect directly the magnetic field from the sample. Instead, the sample move through a system of superconducting detection coils which are connected to the SQUID unit with superconducting wires, allowing the current from the detection coils to be inductively coupled to the SQUID sensor. When properly configured, the SQUID electronics produce an output voltage which is strictly proportional to the current flowing in the SQUID input coil. Hence, the thin film SQUID device operates as an extremely sensitive current-to-voltage convector. A measurement is performed by SQUID-MPMS by moving a sample through the superconducting detection coils, which are located outside the sample chamber and at the center of the magnet. As the sample moves through the coils, the magnetic moments of the sample induce an electric current in the detection coils. Because the detection coils, the connecting wires and the SQUID input coil form a closed superconducting loop. Then, any change of magnetic flux in the detection coils produces a change of the current in the detection circuit.

This current is proportional to the change in the magnetic flux. Since the SQUID works as a highly linear current-to-voltage convector, the current variations in the detection coils produce a corresponding variation in the SQUID output voltage, which is

proportional to the magnetic moment of the sample. In a fully calibrated system, the measuring of voltage variation from the SQUID detector provides a highly precise measurement of the sample's magnetic moment. The system canbe accurately calibrated using a small piece of material having a known mass and magnetic susceptibility.
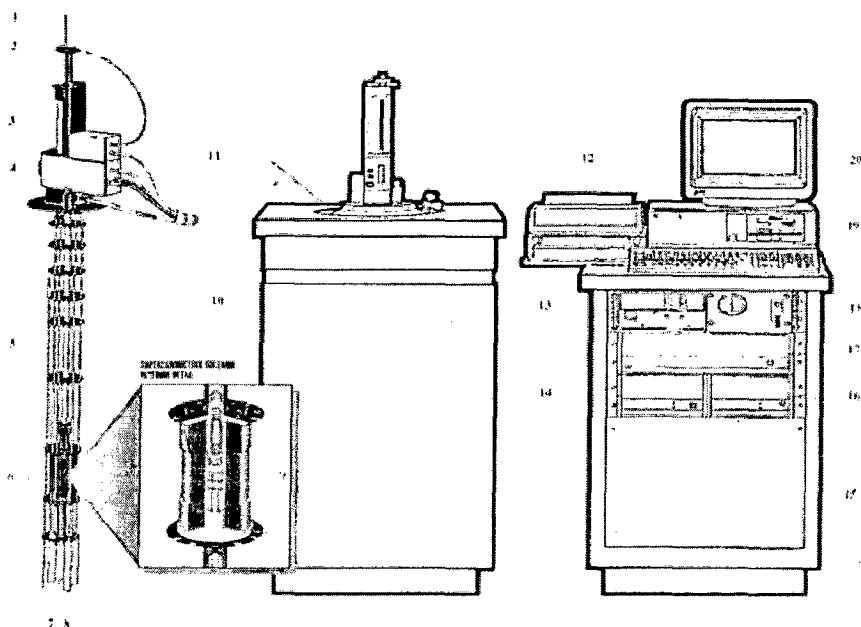
SYSTEM COMPONENTS (superconducting components shown in blue)

1.	Sample Rod	8.	SQUID Capsule with Magnetic Shield	15.	Console Cabinet
2.	Sample Rotator	9.	Superconducting Pick-up Coil	16.	Power Distribution Unit
3.	Sample Transport	10.	Dewar Isolation Cabinet	17.	Model 1822 MPMS Controller
4.	Probe Assembly	11.	Dewar	18.	Gas/Magnet Control Unit
5.	Helium Level Sensor	12.	HP Thinkjet Printer	19.	HP Vectra Computer
6.	Superconducting Solenoid	13.	Magnet Power Supply	20.	Monitor
7.	Flow Impedance	14.	Model 1802 Temperature Controller		

Fig.11. SQUID arrangement

2.4. Experimental Details:

Synthesis of Mn doped ZnO(Zn1-xMnxO) Nanocrystallines by Autocombustion method:

Mn doped ZnO was synthesized by a combustion method from the nitrates of Zn and Mn taken in the appropriate ratio, using glycine as the fuel [30]. Zn and Mn metal powders were taken in stoichiometric amounts and dissolved separately in 4N HNO3 and mixed together. To the above mixed metal nitrate solution,a water solution of 2 moles of glycine per mole of metal was added. The mixed solution was taken in a large crystallizing dish and kept over a hot plate for autocombustion at 473 K. After the complete evaporation of water, a reddish colored thick gel was formed, which was subsequently burnt to give a final brown colored oxide product. The as-synthesized powder samples thus obtained were characterized by powder X-ray diffraction, The powder morphology was studied using a FESEM and EDAX.Magnetization measurements, as a function of magnetic field and temperature, were carried out using a vibration sample magnetometer and SQUID. Electronic absorption spectra were recorded on a UV-vis spectrophotometer,diffuse reflectance spectroscopy and flouroscence spectroscopy.

Initialy Zn(1-x) metal powder was added in 4N HNO3

Then Mn(x) metal powder was added in 4N HNO3

Then both solution was added together

To the above mixed metal nitrate solution,a water solution of 2 moles of glycine per mole of metal was added

The mixed solution was taken in large beaker and kept over hot plate for autocombustion at 473K

The solution was kept on hot plate till it subsequently burn and give a final brown colored oxide product

Characterisation by X-Ray Diffraction on Bruker X-8, FESEM Analysis and EDAX Analysis done on FEI Quanta 200f

36

CHAPTER 3

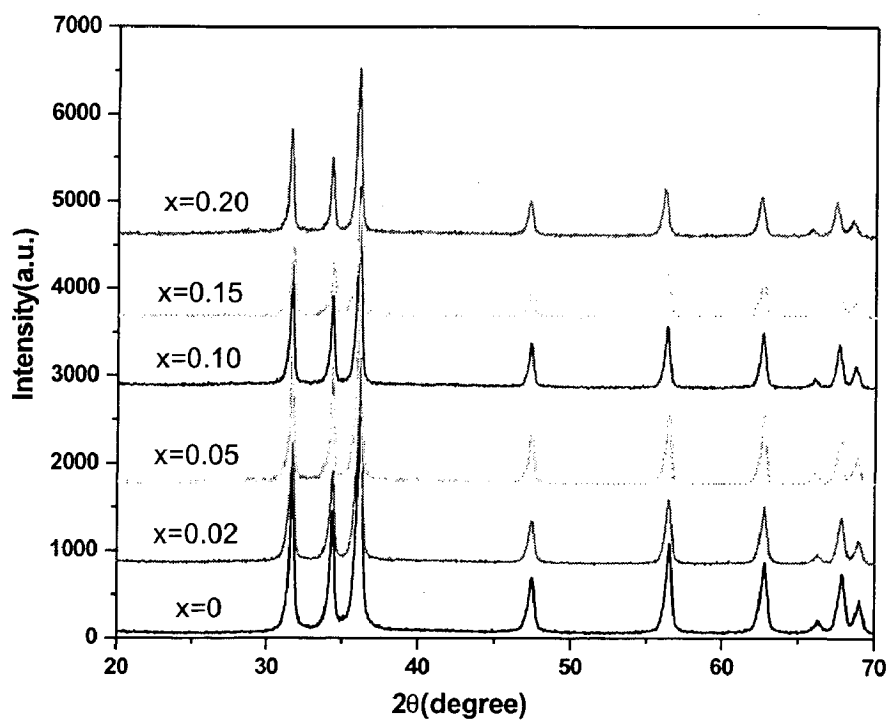# RESULTS AND DISCUSSION

3.1. X-Ray Diffraction results:

Fig.12. Powder X- Ray diffraction patterns of different compositions of
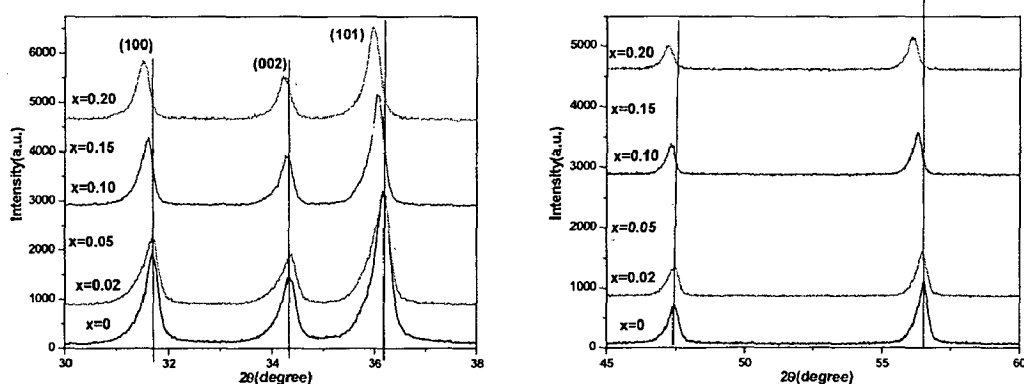
$Zn_{1-x}Mn_xO$ $(0<x<0.20)$

Fig.13. Comparison of the expanded powder XRD patterns of different

compositions in $Zn_{1-x}Mn_xO$ (0 < x < 0.20) in 30°-38° and 46°-80°.The

vertical dashed lines indicate the positions of the indexed reflections from ZnO.

The powder XRD patterns of different $Zn_{1-x}Mn_xO$ (0 <x <0.20) samples are shown in

Fig. 12. The XRD patterns for x > 0 show that the ZnO structure is not disturbed on

substitution. No reflections due to any secondary phase are detected in the XRD patterns.

The width of the reflections increase with increasing Mn content, indicating decreasing

particle (crystallite) size. The average particle sizes were calculated from X-ray line

broadening using the Scherrer formula [31]. A decrease in the average particle size with

increasing Mn content is observed, and similar results are reported in the literature [23].

The average particle size obtaine for different compositions of Zn1−xMnxO are 40, 27,

26, 21, 15, 18 and 15 nm for x = 0, 0.02, 0.05, 0.1, 0.15, 0.2 respectively. The expanded

XRD patterns in the 30–38 degree region, shown in Fig. 2, clearly indicate that the XRD

reflections are shifted to lower 2 thetavalues with increasing concentration of Mn. This is

a proof of the incorporation of Mn ions inside the ZnO crystal lattice. The ionic radius of

38

Zn2+ is 0.60 A°, and that of Mn2+ is 0.66 A° , for four-fold coordination [32]. Hence,

Mn incorporation will lead to an expansion of the ZnO lattice.for (ZnMn)O by various
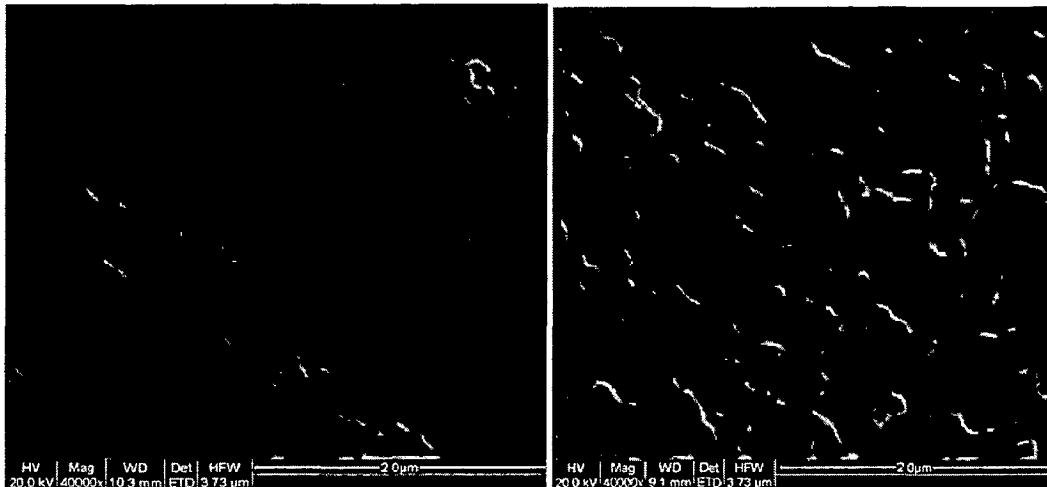
researchers

3.2. FE-SEM Results:
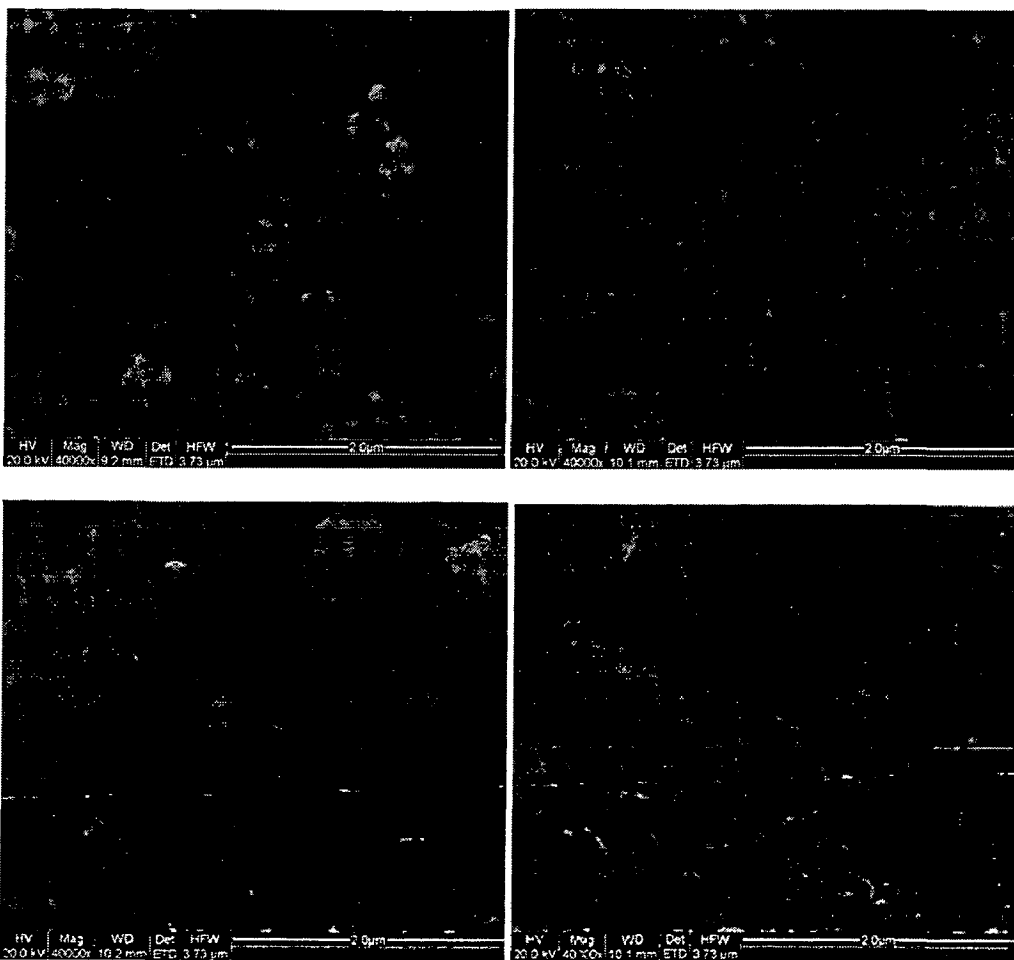
Fig.14.FE-SEM images of as synthesized Mn doped ZnO nanocrystals of different

Compositions as (x=0, 0.02, 0.05, 0.10, 0.15, 0.20) from left to right.

The morphology of the as syntyhesized sample of $Zn_{(1-x)}Mn_xO$ is shown in Fig it can be formulate from FE-SEM images that nanorod formation occur as we increase the composition of Mn concentration in the solution.the diameter of nanowire is approx 70-120 nm.as we have seen that particle size decreases by increasing the concentration of Mn,it can be also conferm from above exist images.
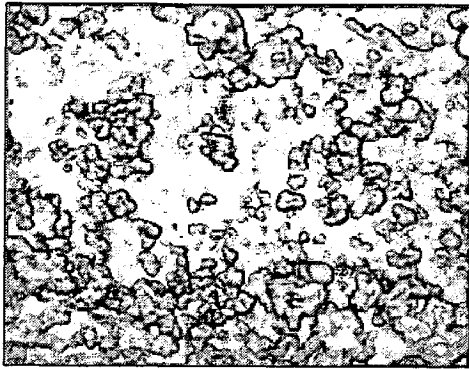
Element	Wt%	At%
OK	05.65	19.63
MnK	01.23	01.25
ZnK	93.11	79.12
Matrix	Correction	ZAF
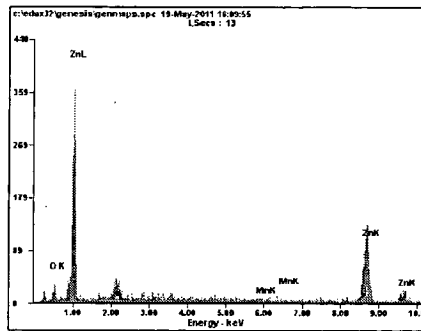
Element	Wt%	At%
OK	14.96	41.73
MnK	01.79	01.45
ZnK	83.25	56.82
Matrix	Correction	ZAF
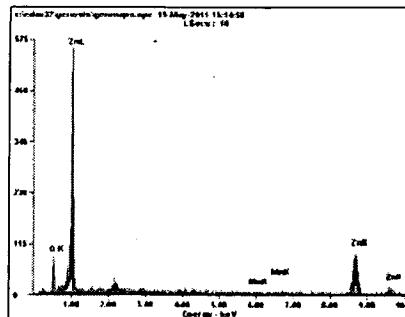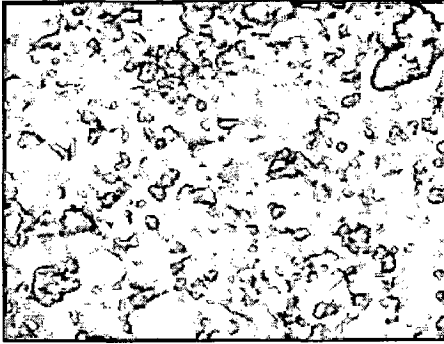
Element	Wt%	At%
OK	05.57	19.31
MnK	03.55	03.58
ZnK	90.88	77.11
Matrix	Correction	ZAF
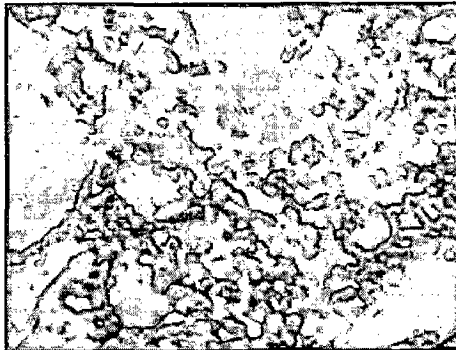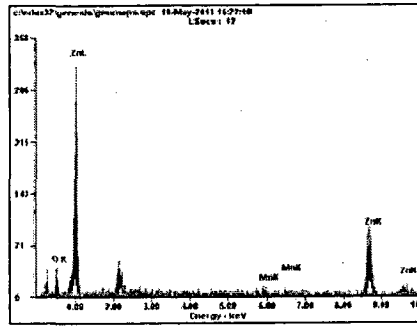
Element	Wt%	At%
OK	07.76	25.15
MnK	11.43	10.78
ZnK	80.80	64.06
Matrix	Correction	ZAF

42
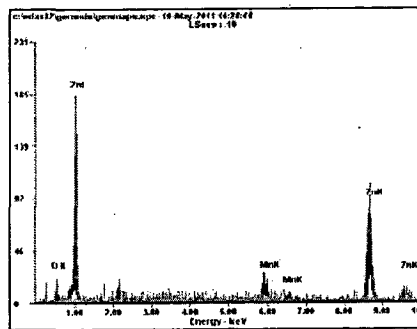
Element	Wt%	At%
OK	05.12	17.86
MnK	07.25	07.37
ZnK	87.62	74.78
Matrix	Correction	ZAF
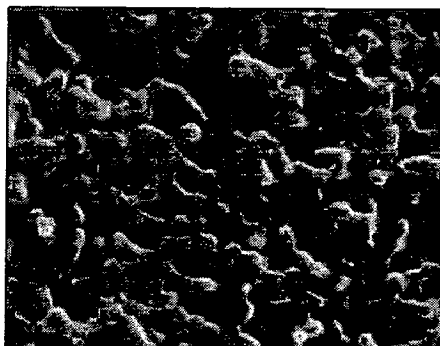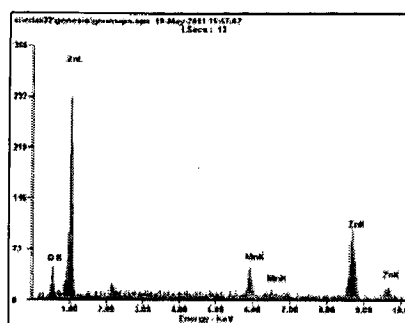
Element	Wt%	At%
OK	11.35	33.67
MnK	14.22	12.28
ZnK	74.43	54.04
Matrix	Correction	ZAF
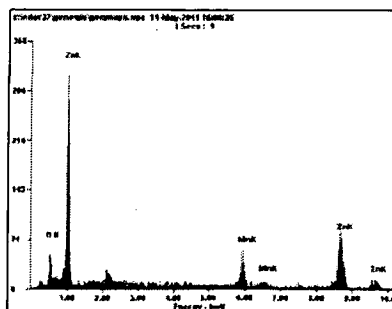
Fig.15.EDAX analysis images of Mn doped ZnO nanocrystals of Mn concentration

(x=0, 0.02, 0.05, 0.10, 0.15, 0.20) respectively

Fig Shows EDXA analysis of Mn doped ZnO nanocrystals withdifferent compositions

The EDXA pattern of different Mn:ZnO nanocrystalswith variable Mn ratios confirmed

Zn,Mn and O elements with different weight percentages.

3.3. OPTICAL PROPERTIES:

We find out the optical properties by using following apparatus:

* UV-vis Spectrophotometer

* UV-vis diffuse reflectance spectrophotometer

* Photolumniscence spectrophotometer

Fig.16. Optical absorption spectra for $Zn_{1-x}Mn_xO$ (x = 0, 0.02, 0.05, 0.15 and 0.2)

Powder samples, recorded at room temperature.

The room temperature optical absorption spectra of the various compositions in $Zn_{1-x}Mn_xO$ are shown in Fig.16. Apart from the band gap transition, other optical absorption features are clearly seen for the doped samples at lower energies. A strong absorption band is seen at 376 for x=0,this band shift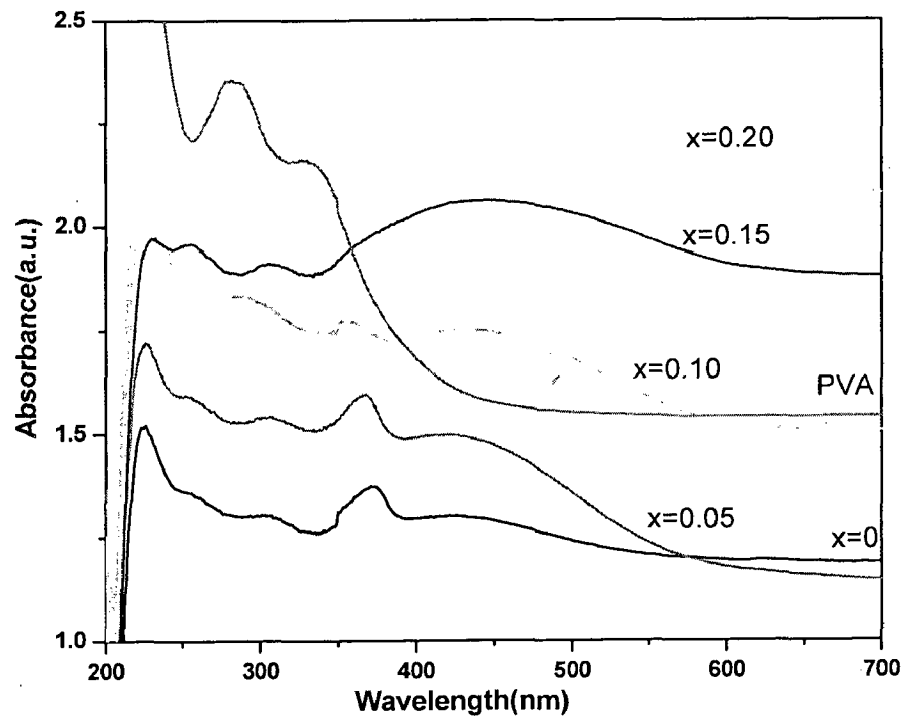ed towards higher wavelength as x increases,for x=0, 0.05, 0.10, 0.15, 0.20 bands are at 376,366,352,333,330.so there is a blue shift observed.This is due to the spin forbidden transition of Mn_{2+} in a tetrahedral environment. Such a type of strong spin forbidden transition is already reported for (ZnMn)O. This is explained in terms of the lattice distortion due to the incorporation of the larger Mn^{2+} ions inside the ZnO lattice. Moreover, an increase in the absorption intensity is observed with increasing x at these wavelengths. A very weak absorption is seen around 426 nm for x=0, which increses as x increases. This feature is not very clear for low doping concentrations, whereas it is slightly visible for the high Mn doped samples. Thus, optical absorption studies confirm the presence of Mn2+ ions in the tetrahedral sites.. The blue shift of the band edge, presence of Mn2+ ions in the tetrahedral sites parameters are some indicators of the incorporation of Mn ions inside the ZnO lattice. The violet emission at 426 nm of the Mn-doped ZnO nanowires is attributed to the electron transition from bottom of the conduction band to zinc vacancy defect energy level. Zinc vacancy defect maybe resulted from the existence of the doping Mn ions.peaks lower than 320 corresponds to PVA (poly vinyl alcohol) which can be seen in the fig.17.
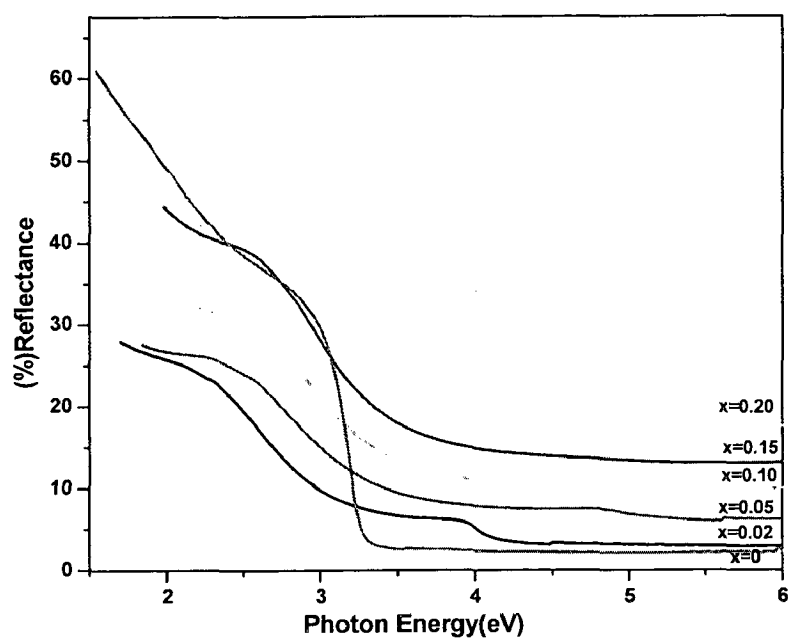
Fig.17.UV-vis diffuse reflectance spectrum of as-synthesized Mn doped ZnO sample of different

composition

Measurements of the optical properties of these Mn doped ZnO nanorods were also

performed.UV-vis diffuse reflectance spectrum of the nanorods was used to determine of

the band gap of these nanorods with increasing Mn concentration.the band gap values for

the doped samples are obtained as 3.33,3.41,3.68,4.01,4.12,4.28eV for

x=0,0.02,0.05,0.10,0.15,0.20 respevtively.The blue shift of the band edge,indicates the

incorporation of mn ions oinside zno lattice.
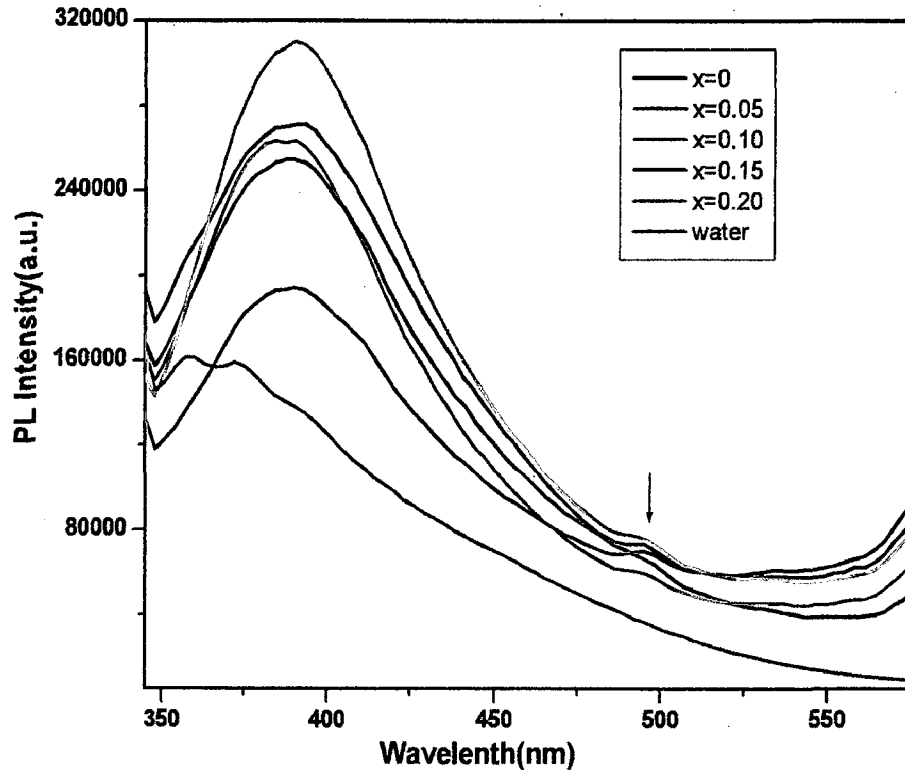
Fig.18. Photolumniscence spectrum of the as-synthesized Mn doped ZnO sample of

Different composition

Fig.18. shows the room temperature PL spectra of the undoped and Mn-doped nanorods

excited by 315 nm UV light using a He–Cd laser as the source. There are three obvious

changes found in the spectrum of the doped as compared with the undoped, which makes

it interesting for discussion. Firstly, the PL spectrum of the undoped consists of a strong

UV band peak at 382 nm. Besides this, a very weak broad green band centred at about

495 nm occurred.

The UV emission band could be related to a near band-edge (NBE) transition of ZnO,

namely the recombination of free excitons through an exciton collision process [24]. The

green emission peak is commonly referred to as a deep-level or trapstate emission. The green band is generally explained by the radial recombination of a photo-generated hole with the electron in a singly ionized oxygen vacancy [25]. It has been reported that due to the excess exciton impurity and crystalline defect scattering, there exists a deep-level emission around 2.6 eV in ZnO nanorods[26, 27]. The almost negligible deeplevel emission in figure (inset) suggests good optical quality of the ZnO nanorods. Secondly, the UV emission peak position ofthe Mn-doped nanorods exhibits blue shift compared with that of the undoped. This is attributed to the shift of the optical band gap in In-doped nanorods [28]. There are more electrons contributed by Mn dopants that take up the energy levels located at the bottom of the conduction band. When the Mn-doped sample is excited with a He–Cd laser at 315 nm, excitons attain energy and move to higher energy levels at the bottom of conduction band than that of the undoped. Radiative recombination of these excitons leads to a blue shift of the UV emission peak. Finally, the intensity of the UV emission peak was suppressed after Mn doping.The suppression in the UV emission intensity in the doped sample is due to the weak exciton Coulomb interaction effect. Indium acts as a scattering centre and generates a Coulomb potential field, which makes excitons ionized because of the loss of the Coulomb interaction effect. As a result, the exciton effect decreases obviously, and the intensity of NBE (near band edge)transitions reduces.

3.4. Magnetic Properties:

Fig.19. shows M–H curves of $Zn_{1-x}Mn_xO$ (x = 0.05,0.2 and 0.25) measured at 10 K. The magnetization curves are almost linear with field strength. However, a closer examination of the magnetization curves, as shown in the insets of Fig. 7 for $Zn_{0.8}Mn_{0.2}O$, reveals that

the sample is paramagnetic at room temperature (M vs. H is linear), whereas it is not truly paramagnetic at 10 K. A large deviation from the expected paramagnetic behavior is observed for higher fields in the 10 K data. This is possible if the sample is superparamagnetic or is a mixture of a major paramagnetic and a minor ferro/ferrimagnetic phases. The absence of a hysteresis loop indicates superparamagnetic behavior.

There are several reports in the literature where Mn-doped ZnO samples are found to be magnetic below 50 K with TC close to 40 K. The large low temperature magnetization in the (ZnMn)O system has been attributed to various effects, such as carrier mediated ferromagnetism, the presence of a ferromagnetic Mn_3O_4 phase , the presence of a secondary Zn substituted spinel $(MnZn)Mn_2O_4$ phase, spin freezing, etc. From the studies on Mn doped ZnO on different substrates, there can also be contributions from the substrate on the observed ferromagnetism. In the present case, since the XRD studies did not show any evidence for the presence of secondary phases, the origin of ferro/ferrimagnetism can be intrinsic or because of defects. However, the presence of secondary phases in very small quantities cannot be ruled out if the amount present is less than the detection limit of XRD. Moreover, the maximum intense peak of the possible spinel-type impurity phase Mn_3O_4 (311) overlaps with the maximum intense peak of ZnO (101), and hence cannot be differentiated from it if present in small amounts. Magnetic characteristics like ferromagnetism at room temperature, ferromagnetism at low temperatures in the samples which are paramagnetic at room temperature, and the absence of ferromagnetism at all temperatures have been reported previously for polycrystalline samples of Mn doped ZnO. Interestingly, the polycrystalline samples are

synthesized by different methods in the different reports, and the results are reproducible whenever the same method is followed. In the present work, the polycrystalline samples are synthesized by autocombustion method. This method has been shown to be suitable for the synthesis of single phase multicomponent oxides .Earlier, we have shown that it is possible to synthesize and stabilize metastable phases of some perovskite oxides by this method, when it is not possible to stabilize these phases by other methods. However, the combustion method is highly susceptible to producing different results, depending on the nature of the fuel used in the reaction as well as the ratio of the fuel to the oxidizer. In the case of Co doped ZnO, it has been shown that both ferromagnetism and paramagnetism at room temperature can be obtained by slightly modifying the synthesis conditions where ferromagnetism was found to be due to the presence of impurity phases. In the present work, it is possible that the observed magnetic characteristics at low temperatures are likely to be either due to the intrinsic behavior from some defect structures created because of the particular synthesis conditions, or due to the presence of minor impurity phases. Further detailed work is required to understand this.
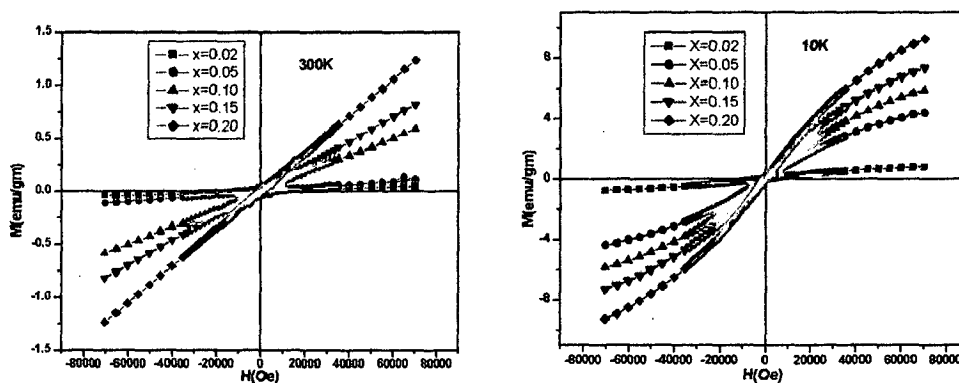

Fig.19. M-H curve of the Mn substituted compositions at 10K and 300K

The magnetization of the different samples is measured as a function of field at room temperature and 10 K as well as a function of temperature at a fixed field strength. All the Mn doped samples were found to be paramagnetic at room temperature. The temperature variations of the magnetization of x=0.02, 0.05, 0.10, 0.15, 0.20 are shown in Fig.20(a). The applied magnetic field in each case was 7000 Oe. All the samples show similar features. A rapid increase in the magnetization is observed below 50 K for all the samples. The inverse of the magnetic susceptibility of different samples are shown in the of Fig.20(b). From the nature of the inverse susceptibility curves, it is likely that the samples are either ferromagnetic or ferrimagnetic at low temperatures. A typical Curie–Weiss behavior is observed above 100 K for the samples. A least squares fit of the linear portion of the curves above 100 K gave a negative Weiss temperature for all samples. The value of T_C is obtained as -300K,-125K,-82K,-24K,0K for x=0.02,0.05,0.10,0.15,0.20 respectively. The high negative values of critical temperature indicate either strong antiferromagnetic or ferromagnetic interactions in these Mn doped samples. An antiferromagnetic nature for the samples can be ruled out from the shape of the susceptibility curves.
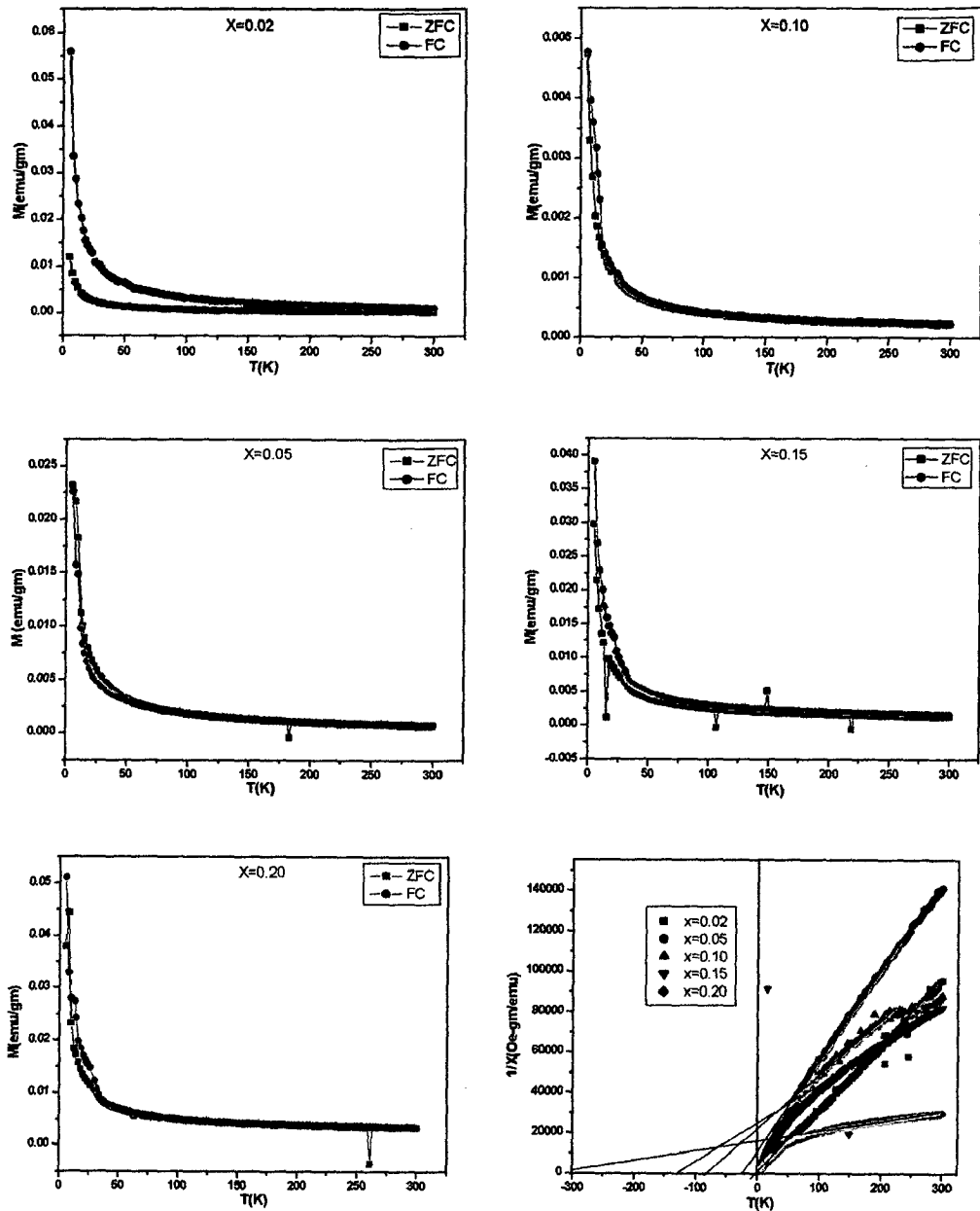
Fig.20. (a) Temperature variation of magnetization (b) Reciprocal susceptibility vs.

temperature of $Zn_{1-x}Mn_xO$ (x =0.02,0.05,0.10,0.15,.020) powder samples.

The results from the magnetic measurements are in agreement with those reported in the literature for $Zn_{1-x}Mn_xO$ samples. Very large negative values of crtical temprature, along with a deviation from linearity below 50 K similar to that observed in the present case, suggesting strong antiferromagnetic couplings. However,considering the large increase in the magnetization below 50 K and the large negative value of the Weiss temperature, it can be considered that the samples are ferrimagnetic.
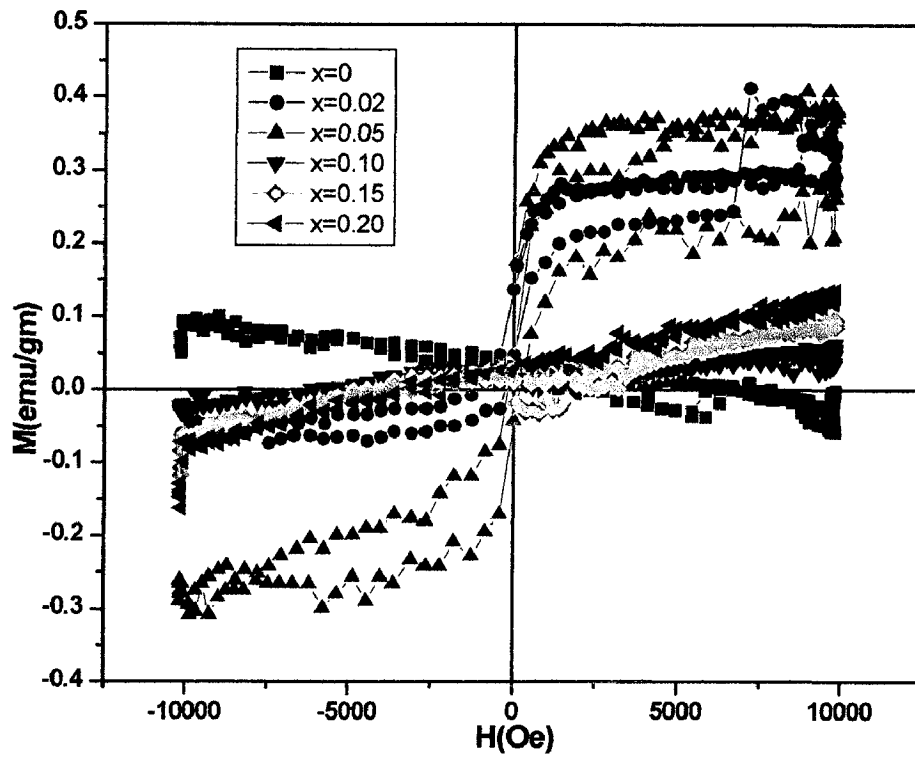

Fig.21.Magnetization of Mn substituted compositions as a function of field at room temperature

The sample with x=0.02,0.05 has the strongest room temperature ferromagnetic properties with a saturation magnetization of 0.35 emu/g,0.30emu/gm and a coercive field of ,1022.4Oe,224.2 Oe at room temperature.we believe that in these samples the concentration of oxygen vacancies plays an important role in mediating the ferromagnectic exchange between Mn ions.for the sample x=0.02,0.05 shows strong ferromagnetism compared to x=0.10,0.15,0.20 despite the fact that these samples contains more Mn ions.we belive that presence of oxygen vacancies is the reason for their long range ferromgnetism .the ferromagnetic properties of this sample are the strongest. In addition, nearly all of the possible Mn-based binary and ternary oxide candidates are antiferromagnetic , According to RKKY theory, the magnetism is due to the exchange interaction between local spin-polarized electrons (such as the electrons of Mn^{2+} ions) and conductive electrons. This interaction leads to the spin polarization of conductive electrons, and then throughout by the interaction between the conductive electrons. Therefore the long-range exchange interaction makes all of the Mn^{2+} ions have the same spin direction. As a result, the material exhibits ferromagnetism. In our experiment, more local spin-polarized electrons and conductive electrons will be provided with an increasing additional quantity of Mn^{2+} .Therefore, the ferromagnetic properties of x=0.10,0.15,0.20 are smaller than that of x=0.02,0.05. A typical diamagnetic behavior was observed. The diamagnetic behavior of ZnO is due to the paired electrons of its d orbital, which is responsible for the absence of a permanent net magnetic moment per atom. Then, when electrons are paired together, their opposite spins cause the magnetic fields to cancel with each other. Accordingly, when an applied magnetic field is acting on this atom slightly unbalances their orbiting electron and

creates small magnetic dipoles within the atoms which oppose the applied field. This action produces a negative magnetic effect. Observed paramagnetic behavior can be attributed to the actual incorporation of Mn ions into the otherwise diamagnetic ZnO structure; although the precipitation of an anti-ferromagnetic phase can not be ruled out. Figure 40 evidences a clear discrepancy for a pure paramagnetic behavior, particularly at low magnetic fields, for the sample synthesized at 'x' = 0.10, 0.15, 0.20. A very weak coercivity was observed in this case (Hc ~ 25 Oe) Furthermore, the almost linear field dependence of magnetization within the applied magnetic field range is considered typical of an antiferromagnetic compound. The corresponding ferromagnetism could be explained by one of the Goodenough-Kanamori-Anderson (GKA) rules, which suggests the possibility of a weak ferromagnetism in the case of a 90°-exchange interaction between (half)-filled orbitals. The magnetic behavior can also be a consequence of the indirect exchange interaction through the carrier-mediated model. Generally, it has been reported that the magnetic ordering in a diluted magnetic system could be explained by the indirect exchange interaction through the spinpolarized carrier. The existence of the spin-polarized carrier in our samples could be verified by the measurement of either quantum Hall effect or magnetoresistance effect.

CONCLUSION

Single phase $Zn_{1-x}M_xO$ (0 $<$x <0.25) nanocrystals have been synthesized using a simple combustion method. With the increasing content of Mn, lattice parameters of doped ZnO increase due to the larger ionic radius of Mn^{2+}.Optical absorption investigations reveal the presence of Mn^{2+}in tetrahedral coordination, possibly due to the substitution of Mn for Zn in the ZnO lattice. All samples are paramagnetic at room temperature, and the susceptibility data give evidence for strong antiferromagnetic interactions and room temperature ferromagnetism also obtained for some low Mn doped ZnO. A large increase in the magnetization below 50 K and nonlinear M – H behavior at 12 K indicate that the samples are ferrimagnetic at low temperatures. However, the presence of small fractions of other ferromagnetic, impurities in the paramagnetic samples cannot be ruled out.

REFERENCES:

[1] Ohno. F. Matsukura and Y. Ohno. JSAP International. Vol 5 (2002), 4

[2] S.J. Pearton, C.R. Abernathy, D.P. Norton, A.F. Herbard, Y.D. Park, L.A. Boather, J.D. Baudai, Mat Sc. And Engg., Vol R40 (2003),137

[3] S. Das Sarma, American Scientist, Vol 89 (2001) 516

[4] H. Ohno, Science, Vol 281 (1998), 951

[5] Mauger A and Godart C 1986 *Phys. Rep.* 141 51

[6] H-W. Zhang, E-W. Shi, Z-Z. Chen, X-C. Liu, Bing Xiao., Vol 137 272-274 (2006).

[7] H. Ohno, Science, Vol 281 (1998), 951

[8] K. Ueda, H. Tabata, T. Kawai. Appl. Phys. Letters, Vol 79, 988-990 (2001)

[9] S.W. Jung, S. J. An, and Gyu- Chul Yi. Appl. Physic. Letters, vol 80, 4561-4563 (2002).

[10] H. Katayama-Yoshida, K Sato / Jpn. J. Appl. Phys B 39 (2000) L555.

[11] Y. W. Heo, M. P. Ivill, K. Ip, D.P. Norton, S. J. Pearton, J. G. Kelly, R. Rairigh, A. F. Hebard, T. Steiner., Appl. Phys. Letters, Vol 84, 2292-2294, (2004).

[12] N. Theodoropoulou, G. P. Barera, V. Misra, P. LeCalir, J. Philip, J. S. Moodera, B. Satapi, and T. Som (unpiblisched).

[13] L. Yan, C. K. Ong, X. S. Rao., J. Appl. Phys., Vol 96, 508-511 (2004)

[14] Gamelin et al J. Am. Chem. Soc., Vol 126, 9387-9398 (2003)

[15] S.N. Khanna, B.K. Rao, P. Jena, M. Knickelbein, Chemical Phys. Letts., 378 (2003) 374

[16] S.J. Pearton et al. / Physica B 340–342 (2003) 39–47

[17] M. Baibich, J. Broto, A. Fert, F. v. Dau, F. Petroff, P. Etienne, G. Greuzet, A. Friederich, and J. Chazelas, "Giant Magnetoresistance of (001)Fe/(001)Cr Magnetic Superlattices," Phys. Rev. Lett. Vol 61, 2472 (1988).

[18] G. Binash, P. Grunberg, F. Saurenbach, and W. Zinn, "Enhanced Magnetoresistance in Layered Magnetic Structures with Antiferromagnetic Interlayer Exchange," Phys. Rev. B. Vol 39, 4828 (1989).

[19]. S. S. P. Parkin, Z. G. Li, and D. J. Smith, "Giant Magnetoresistance in Antiferromagnetic Co/Cu Multilayers," Appl. Phys. Lett. Vol 58, 2710 (1991); S. S. P. Parkin, R. Bhadra, and K. P. Roche, "Oscillatory Magnetic Exchange Coupling Through Thin Copper Layers," Phys. Rev. Lett. Vol 66, 2152 (1991).

[20] B. Dieny, V. S. Speriosu, S. S. P. Parkin, and B. A. Gurney, "Giant Magnetoresistance in Soft Ferromagnetic Multilayers," Phys. Rev. Vol B 43, 1297 (1991).

[21] S. A. Wolf, A. Y. Chtchelkanova, D. M. Treger, IBM Journal of Research and Development. Spintronic Vol 50 Number 1, 2006

[22] http://www.pcguide.com/ref/hdd/op/heads/techGMR-c.html

[23] Datta and Das, Appl. Phys. Lett., Vol 56, (1990) 665

[24] Zutic, J. Fabian, S. D. Sarma. Reviews of Modern Physics. Vol 76, 2004

[25] D. Peiteado. Norton, *et al.*, Appl. Phys. Letters, Vol 83 5488-5490.

[26] Dietl Thota, Ohno H, Matsukura F, Cibert J and Ferrand D 2000 Science 287 1019.

[27] D. Schwartz, N. S. Norberg, Q. P. Nguyen, J. M. Parker, and D. Gamelin., J. Am. Chem. Soc. Vol 125, 13205-13218 (2003).

[28] Sasanka Deka, P.A. Joy.2003 j.solid state comm.217 (778)

[29] Ü. Özgür, Ya. I. Alivov, C. Liu, A. Teke, M. A. Reshchikov, S. Doğan, V. Avrutin, S. J. Cho, and H. Morko J. Appl. Phys. Vol 98, 041301 (2005).

[30] T. Fukumura, Z. Jin, A. Ohtomoto, H. Koinuma, M. Kawasaki. Appl. Phys. Lett., vol 75 (1999), 3366.

[31] T. Fukumura, Z. Jin, M. Kawasaki, T. Shono, T. Hasegawa, S. Koshihara, and H. Koinuma., Appl. Phys. Lett., vol 78, 958 (2001).

[32] H-W. Zhang, E-W. Shi, Z-Z. Chen, X-C. Liu, Bing Xiao., Vol 137 272-274 (2006).

[33] X.M. Cheng and C. L. Chien., J. Appl. Phys. Vol 93, 7876 (2003).

[34] K. Ueda, H. Tabata, T. Kawai. Appl. Phys. Letters, Vol 79, 988-990 (2001)

[35] R. K. Zheng, H. Liu, and X. X. Zhang, V. A. L. Roy, A. B. Djurišic. Appl. Phys. Letters. Vol 85, 2589-2591 (2004).

[36] S.W. Jung, S. J. An, and Gyu- Chul Yi. Appl. Physic. Letters, vol 80, 4561-4563 (2002).

[37] Y. W. Heo, M. P. Ivill, K. Ip, D.P. Norton, S. J. Pearton, J. G. Kelly, R. Rairigh, A. F. Hebard, T. Steiner., Appl. Phys. Letters, Vol 84, 2292-2294, (2004).

[38] N. Theodoropoulou, G. P. Barera, V. Misra, P. LeCalir, J. Philip, J. S. Moodera, B. Satapi, and T. Som (unpiblisched).

[39] L. Yan, C. K. Ong, X. S. Rao., J. Appl. Phys., Vol 96, 508-511 (2004)

[40] Gamelin et al J. Am. Chem. Soc., Vol 126, 9387-9398 (2003)

[41] J. H. Kim, H. Kim, D. Kim Y. E. Ihm, W. K. Choo. J. Appl. Phys. Vol 92, 6066-6071 (2002)

[42] H. J. Lee and S-Y. Jeong, C-R. Cho, C-H. Park. Appl. Phys Letters. Vol 81, 4020-4022 (2002)

[43] D. Peiteado. Norton, *et al.*, Appl. Phys. Letters, Vol 83 5488-5490.

[44] K. Ando, H. Saito, Zhengwu Jin, T. Fukumura, M. Kawasaki, Y. Matsumoto, H. Koinuma., J. Appl. Phys., Vol 78, 2700 (2001).

[45] Z. Jin et al., J. Appl. Phys., Vol 78, 3824-3826 (2001).

[46] Tawari, C. Jin, A. Kvit, D. Kumar, J. F. Muth, J. Narayan. Solid State Comm., Vol 121, 371 (2002).

[47] P. Radovanovic, and D. Gamelin., Phys. Rev. Lett Vol 91, 157202-1 (2003)

[48] D. Schwartz, N. S. Norberg, Q. P. Nguyen, J. M. Parker, and D. Gamelin., J. Am. Chem. Soc. Vol 125, 13205-13218 (2003).

[49] L. Spanhel, M. Anderson., J. Am. Chem. Soc. Vol 113, 2826-2833, (1991)

[50] H. Zhou *et al.* Appl. Phys. Lett. Vol 80, 210-212, 2002

[51] Meulenkamp, E. A. J. Phys. Chem. B. Vol. 102, 5566-5572, (1998)

[52] J. Daniel Bryan, D. A. Schwartz, and D. Gamelin. J. Nanotechnolgy

[53] E. Hosono, S. Fujihara, T. Kimira and H. Imai, J. Sol-Gel Science and Technolgy, Vol 29, 71-79, 2004

[54] N. Yao, Z. L. Wang, "Handbook Microscopy for Nanotechnology", p 427

[55] L. E. Brus, J. Chem. Phys. Vol 79, 5566 (1983)

[56] L. E. Brus, J. Chem. Phys. Vol 80, 4403 (1984)

[57] L. E. Brus, J. Chem. Phys. Vol 90, 2555 (1986)

[58] Y. Kayanuma, Phys. Rev. B, Vol 42, 7253 (1990)

[59] Al. L. Efros and A. L. Efros, Sov. Phys. Semicond. Vol 16, 772 (1982)

[60] S. Monicone, R. Tufeu, and A. V. Kanaev. J. Phys. Chem. B. Vol 102, 2854-2862 (1998)

[61] N. S. Pesika, Z. Hu, K. J. Stebe and P. Searson. J. Phys. Chem. B. Vol 106, 6985-6990 (2002)

[62] N. S. Pesika, K. J. Stebe and P. Searson, Adv. Mater. Vol 15, 1289-1291 (2003)